

Centre de Physique Théorique\* - CNRS - Luminy, Case 907  
F-13288 Marseille Cedex 9 - France

## PHENOMENOLOGICAL APPROACH TO UNPOLARIZED AND POLARIZED PARTON DISTRIBUTIONS AND EXPERIMENTAL TESTS

Claude BOURRELY and Jacques SOFFER

### Abstract

We recall our recent description of quark parton densities of the proton at  $Q^2 = 4\text{GeV}^2$  in terms of Fermi-Dirac distributions parametrized with very few free parameters. We have also proposed some simple assumptions to relate unpolarized and polarized quark parton densities which lead to a fair description of the spin-dependent structure functions  $xg_1^p(x, Q^2)$  and  $xg_1^n(x, Q^2)$  at low  $Q^2$ . We will show the predictions we obtain after a straight-forward DGLAP  $Q^2$  evolution and comparison in a much broader  $x$  and  $Q^2$  range, with several recent and accurate deep-inelastic scattering data. In particular, we will see that we get an excellent agreement with the sharp rise of  $F_2^{ep}(x, Q^2)$  for small  $x$ , recently observed at HERA. Finally, we give several predictions for lepton pair and gauge boson production in  $pp$  and  $pn$  collisions at high energies which will be tested in the future at RHIC.

Key-Words : polarized parton densities, deep-inelastic scattering, hadronic collisions.

Number of figures : 31

February 1995  
CPT-95/P.3160

anonymous ftp or gopher: cpt.univ-mrs.fr

---

\*Unité Propre de Recherche 7061

# 1 Introduction

Deep-inelastic lepton-hadron scattering is the basic source of our knowledge on quark parton densities of the proton and an enormous amount of data has been accumulated over the last twenty years or so. It allows to test rather accurately our picture of the nucleon structure at short distances. With the advent of HERA, a new kinematical range is now accessible in  $x$  down to  $10^{-4}$  and in  $Q^2$  up to  $10^4 GeV^2$ , which will be extremely useful for the physics analysis at future hadron colliders. Besides the determination, for each flavor  $u, d, s$ , etc..., of the valence quarks which dominate, say for  $x \geq 0.1$ , and of the sea quarks (or antiquarks) which dominate in the small  $x$  region, it is very important to extract the correct gluon distribution. This is because, first it also prevails at low  $x$  and second, it plays a crucial role in the  $Q^2$  evolution for testing perturbative QCD.

Let us now briefly review the main points of our approach. Since quarks carry a spin-1/2, it is natural to consider that the basic distributions are  $xq_i^\pm(x, Q^2)$  corresponding to a quark of flavor  $i$  and helicity parallel or antiparallel to the proton helicity. Recently we have proposed [1] a simple description of these quark densities in terms of Fermi-Dirac distributions with very few free parameters, which were determined from the data at  $Q^2 = Q_0^2 = 3GeV^2$ . This statistical physical picture for the nucleon structure functions is largely motivated by the importance of the Pauli exclusion principle, which can be advocated to explain several experimental features, as discussed in ref.[1]. The fact that there is also some experimental evidence for the existence of simple relations between unpolarized and polarized quark parton densities has allowed us to reduce to *four*, the total number of independent distributions, i.e. two for valence quarks  $xu_{val}^\pm(x, Q_0^2)$  and two for sea quarks (or antiquarks)  $xu_{sea}^\pm(x, Q_0^2)$ . In this approach, the corresponding four  $d$  quark densities  $xd_{val}^\pm(x, Q_0^2)$  and  $xd_{sea}^\pm(x, Q_0^2)$  are related to the four  $u$  quark densities mentioned above and similarly for the  $s$  quark (or antiquark) densities. Concerning the gluon distribution  $xG(x, Q^2)$ , for the sake of consistency, at  $Q^2 = Q_0^2$  we have used a Bose-Einstein expression. As we will see, on the one hand, it is fully consistent with our present knowledge of  $xG(x, Q^2)$  extracted from deep-inelastic scattering data and, on the other hand, it leads to the correct  $Q^2$  evolution of the structure functions. Actually, one of the main purpose of this paper is to show that, starting from our simple scheme, which is in very good agreement with all spin-average and

spin-dependent structure functions for  $Q^2$  near  $Q^2 = Q_0^2$ , one gets, after a standard QCD  $Q^2$  evolution, *predictions* fairly consistent with the data, in a much broader  $x$  and  $Q^2$  range.

The paper is organized as follows. In section 2, we briefly review and update our parametrization of the quark (antiquark) parton and gluon densities at  $Q^2 = Q_0^2$  and show their  $Q^2$  evolution. In section 3, the predictions we obtain for the spin-average structure functions  $F_2^{\ell p}(x, Q^2)$  with  $\ell = e, \mu$  and  $xF_3^{\nu N}(x, Q^2)$  are compared with various deep-inelastic scattering data, including the recent results from HERA. We also give our predictions for the  $W$  production cross section at the Tevatron and for the asymmetries in Drell-Yan lepton pair production and  $W$  production in  $pp$  and  $pn$  collisions, which are sensitive to the flavor asymmetry of light sea quarks in the proton. Section 4 is devoted to the discussion of quark and gluon helicity distributions at  $Q^2 = Q_0^2$  and the comparison of our predictions with the most recent data on the spin-dependent structure functions  $xg_1^p(x, Q^2)$  for proton,  $xg_1^n(x, Q^2)$  for neutron and  $xg_1^d(x, Q^2)$  for deuteron. We also discuss their  $Q^2$  evolution and give our predictions for single and double helicity asymmetries for  $pp$  collisions at RHIC. Finally, in section 5 we consider the *transversity* distribution of quarks (antiquarks) denoted by  $h_1^q(x)$ , which can be extracted from Drell-Yan lepton pair and  $Z$  production in  $pp$  collisions with both proton beams transversely polarized. We give our concluding remarks in section 6.

## 2 Quark (antiquark) parton and gluon distributions

Let us first consider the distributions at  $Q^2 = Q_0^2 = 3GeV^2$ . For valence quarks we have two basic densities  $xu_{val}^{\pm}(x, Q_0^2)$  which are expressed in terms of Fermi-Dirac distributions of the form

$$xp(x, Q_0^2) = \frac{a_p x^{b_p}}{\exp[(x - \widetilde{x}_p)/\bar{x}] + 1} \quad (1)$$

where  $\widetilde{x}_p$  plays the role of the "thermodynamical potential", which is a constant for each quark species and  $\bar{x}$  is the "temperature" which is the same for quarks, antiquarks and gluons. This *universal constant* is independent of the parton helicity. We use a fitting procedure slightly different from that of

ref.[1] which is based on the most accurate neutrino data from CCFR [2, 3] for  $x F_3^{\nu N}(x, Q^2)$ , which has pure valence contributions, and also gives the antiquark distribution at  $Q^2 = 3 GeV^2$  (see below). Of course we will check the good agreement with the most recent NMC data[4] for  $F_2^p(x, Q^2)$  and  $F_2^n(x, Q^2)$  at  $Q^2 = 4 GeV^2$ . It yields the following universal temperature and four free parameters entering in eq.(1)

$$\bar{x} = 0.092, b_+ = 0.354, b_- = 0.738, \tilde{x}_+ = 0.510, \tilde{x}_- = 0.231 . \quad (2)$$

Clearly one has

$$x u_{val}(x, Q_0^2) = x u_{val}^+(x, Q_0^2) + x u_{val}^-(x, Q_0^2) , \quad (3)$$

and, as we argued in ref.[1], we take

$$x d_{val}(x, Q_0^2) = 2 x u_{val}^-(x, Q_0^2) . \quad (4)$$

$a_{\pm}$  are not free parameters, but two normalization constants for the valence quarks in the proton. We note that the values of these parameters (see eq.(2)) are different from those of ref.[1] and correspond to a better fit of  $x F_3^{\nu N}(x, Q_0^2)$  at large  $x$ , as shown in Fig.1a. In particular we now find that the temperature  $\bar{x}$  is slightly smaller than what we found in ref.[1]. We also note that the potentials  $\tilde{x}_+$  and  $\tilde{x}_-$  for the two different helicity states have numerical values in the ratio  $\sqrt{5}$  which is smaller than what we found in our previous analysis. As expected  $\tilde{x}_+ > \tilde{x}_-$ , so  $u_{val}^+$  dominates over  $u_{val}^-$ .

We now turn to antiquarks (or sea quarks) and for  $x \bar{u}^{\pm}(x, Q_0^2)$  we use the same expression eq.(1), but in this case the potential has a smooth  $x$  dependence. This might reflect the fact that in this statistical description of the proton, we must consider the existence of two phases : a gaz corresponding to valence quarks, which dominates at large  $x$ , with a constant potential and a liquid corresponding to sea quarks (or antiquarks), which prevails at small  $x$ , with a potential slowly varying in  $x$ , that we take linear in  $\sqrt{x}$ . In addition, we expect quarks and antiquarks to have opposite potentials, consequently the gluon which produces  $q\bar{q}$  pairs has a zero potential (see below). Moreover since in the process  $G \rightarrow q_{sea} + \bar{q}$ ,  $q_{sea}$  and  $\bar{q}$  have opposite helicities, the potentials for  $u_{sea}^+$  (or  $\bar{u}^+$ ) and  $\bar{u}^-$  (or  $u_{sea}^-$ ) will be opposite. So we take

$$\tilde{x}_{\bar{u}^+} = -\tilde{x}_{\bar{u}^-} = x_0 + x_1 \sqrt{x} . \quad (5)$$

For the  $\bar{d}$  distributions, we assume no polarization at  $Q_0^2$  so we take

$$x\bar{d}^+(x, Q_0^2) = x\bar{d}^-(x, Q_0^2) = x\bar{u}^-(x, Q_0^2) , \quad (6)$$

in accordance to eq.(4). Since when  $x \rightarrow 0$ , from Pomeron universality, one expects  $x\bar{u}(x, Q_0^2) = x\bar{d}(x, Q_0^2) \neq 0$ ,  $\bar{a}_-$  is not a free parameter and will be fixed by this constraint. This implies in addition  $\bar{b}_+ = \bar{b}_-$ . For the strange quark (or antiquark) distributions, we also assume they are unpolarized and we take, in agreement with neutrino deep-inelastic scattering data,

$$xs(x, Q_0^2) = x\bar{s}(x, Q_0^2) = \frac{1}{4} (x\bar{u}(x, Q_0^2) + x\bar{d}(x, Q_0^2)) . \quad (7)$$

Therefore the antiquarks depend on *four* free parameters which are different from those determined in ref.[1], that is

$$\bar{a}_+ = 0.0185, \quad \bar{b}_+ = \bar{b}_- = -0.340, \quad x_0 = 0.219 \quad \text{and} \quad x_1 = -0.406 . \quad (8)$$

We show in Fig.1b the result of our fit for  $x\bar{q}(x)$  at  $Q^2 = 3\text{GeV}^2$ . The NMC data for  $F_2^p$  and  $F_2^n$  which involve both valence quarks and sea quarks have also been used to test the correct determination of our four basic quark (antiquark) densities and the results are shown in Figs.2a,b.

For comparison, we have also given in Figs.1 and 2 the curves obtained by using the MRS(A) parametrization at  $Q^2 = 4\text{GeV}^2$ , taken from ref.[6].

Finally concerning the gluon distribution, for the sake of consistency, we use a Bose-Einstein expression given by

$$xG(x, Q_0^2) = \frac{a_G x^{b_G}}{e^{x/\bar{x}} - 1} \quad (9)$$

with a vanishing potential and the same temperature  $\bar{x}$  as we discussed above. It is also reasonable to assume that for very small  $x$ ,  $xG(x, Q_0^2)$  has the same dependence as  $x\bar{q}(x, Q_0^2)$ , so we will take  $b_G = 1 + \bar{b}$ , where  $\bar{b} = \bar{b}_\pm$  is given in eq.(8). So except for the overall normalization  $a_G$ ,  $xG(x, Q_0^2)$  has no free parameter. From the momentum sum rule, we find  $a_G = 13.146$ . For the sake of completeness, we also need to specify the gluon polarization for which there is no data at all, but we will make some simple speculations in section 4.

To summarize, this statistical approach of the nucleon allows the construction of *all* quark, antiquark and gluon distributions in terms of simple

expressions which depend on *nine* free parameters. We gave some comprehensive arguments about the physical meaning of these parameters for which we don't have yet a full understanding. This small number of free parameters has been determined from deep-inelastic scattering data [2, 3, 4] at low  $Q^2$ . Then, by means of a straightforward DGLAP [5]  $Q^2$  evolution, we will compare our predictions with the existing data in a broad kinematical range of  $x$  and  $Q^2$ , in order to test scaling violations and the dynamics implied by perturbative QCD. This approach contrasts with other methods presented in the literature [6, 7] where one performs a global analysis with parton densities expressed in terms of a large number of free parameters, of the order of twenty, which are fixed by fitting several hundreds of data points. Notice that they are only dealing with spin-average distributions and it is necessary to introduce a new set of parameters to describe spin-dependent structure functions [8]. Before closing this section, we would like to show the  $x$ -shapes of various unpolarized parton distributions at  $Q^2 = Q_0^2 = 3\text{GeV}^2$  and  $Q^2 = 20\text{GeV}^2$ , after a standard  $Q^2$  evolution. As already mentioned in ref.[1], we have used a numerical solution [9] of the DGLAP equations. We display in Fig.3 the  $u$  and  $d$  (valence + sea) quark distributions and also the corresponding antiquark distributions at two different values of  $Q^2$ . The gluon density  $xG(x, Q^2)$  is shown in Fig.4. In the next section we will compare the results of our calculations, using these parton densities, with several pieces of existing experimental data and we will also give our predictions for future measurements.

### 3 Experimental tests for unpolarized parton densities

Since all parton densities have been determined, in order to test our approach, we can now proceed and calculate several physical quantities measured either in deep-inelastic scattering or in hadronic collisions. We will first study various structure functions in deep-inelastic scattering and then turn to hadronic processes with a special emphasize for testing the flavour asymmetry of the light sea quarks, i.e.  $\bar{u} \neq \bar{d}$ .

### 3.1 Deep-inelastic scattering

We first consider the high statistics  $\nu N$  deep-inelastic scattering CCFR data [2] from which one extracts  $x F_3^{\nu N}(x, Q^2)$ . As noticed above, this structure function gives a precise measurement of the isolated valence quark contributions and we show in Fig.5 the results of our calculations. These neutrino data were obtained on a iron target, but we don't think we can treat properly the nuclear effects. Therefore we have not tried to make any heavy nuclear target corrections which are known to be less important for  $x F_3^{\nu N}$  than for  $x F_2^{\nu N}$  which contains the sea quark distributions. However in order to get the remarkable agreement displayed in Fig.5 we had to shift up by 4% our theoretical predictions.

Next we turn to  $\mu p$  and  $ep$  deep-inelastic scattering for which several experiments have yielded a large number of data points on the structure function  $F_2^{\ell p}(x, Q^2)$ . First we will analyze the fixed target measurements which cover the limited kinematical region  $0.0125 \leq x \leq 0.75$  and  $3 \leq Q^2 \leq 230 GeV^2$ , one obtains by combining the NMC data [10] and the BCDMS data [11]. Our predictions are now compared with the data in Figs.6a,b but in this case we need to shift up by 12% the theoretical curves. The description of the data is rather impressive except at  $x = 0.75$  for  $Q^2 < 10^2 GeV^2$  where the BCDMS data lie above the prediction. This is surprizing to us, because this kinematic region is dominated by valence quark contributions which are in perfect agreement with the measurement of  $x F_3^{\nu N}$  at large  $x$ , as we have seen in Fig.5.

We now turn to the very recent measurements of  $F_2^{ep}$  at Hera from the Zeus Collaboration [12] and the H1 Collaboration [13]. It is important to note that these data are essentially in the low  $x$  region which is dominated by the sea quark densities. The behaviour of  $F_2^{ep}$  is therefore mainly constrained by the parameters given in eq.(8) and specially by  $\bar{b} = -0.340$ , which was fixed by the steep behaviour of  $x\bar{q}(x)$  at low  $Q^2$ , as shown in Fig.1b. So this rise of the Hera data in the small  $x$  region was predictable from the CCFR measurement of  $x\bar{q}(x)$  and no new parameter is required. This is not what was claimed in ref.[6] where  $\lambda = -0.3$  was introduced at posteriori. Our predictions, with *no overall normalization factor*, are compared with the data in Figs.7a, b and c and the agreement is absolutely remarkable. From these new measurements of  $F_2^{ep}$ , by analyzing the scaling violations, it is possible to improve our knowledge on the gluon density in the low  $x$  region.

Going back to Fig.4, we see that  $xG(x, Q^2)$  increases very rapidly, and as we expect, it is fairly consistent with the distribution extracted at  $Q^2 = 20\text{GeV}^2$  from the Zeus Collaboration [14].

So far we have tested our parton densities in a kinematical region with  $Q^2 > Q_0^2 = 3\text{GeV}^2$  and we have seen that one gets a very satisfactory description of all deep-inelastic structure functions. Clearly this confirms the success of the DGLAP  $Q^2$  evolution for values above our starting point at  $Q^2 = Q_0^2$ . Without trying to make a systematic study of the low  $Q^2$ , low  $x$  region in electroproduction, we would like to show what we obtain for  $Q^2 < Q_0^2$ , corresponding also to rather small  $x$  values. In this region there are already some data from NMC [10], also earlier from SLAC [15] and some preliminary results from the FNAL muon scattering E665 experiment [16]. Just for illustration, we compare in Figs.8a and b our predictions with the NMC and SLAC data for  $Q^2 \geq 1\text{GeV}^2$  and our curves for  $x \leq 0.007$  are given to be confronted with the final E665 data. For  $Q^2 < 1\text{GeV}^2$  the understanding of the electroproduction structure functions certainly lies outside a perturbative QCD framework and involves other dynamical concepts [17].

## 3.2 Hadronic processes

As we discussed in ref.[1], one of the main features of our approach is the flavor symmetry breaking of the light sea quarks which was first recognized in ref.[18] following an earlier NMC measurement [19]. Here we will stress again the importance of this fact, we will indicate how one can confirm it and we will see where to expect  $\bar{u}(x, Q^2) \neq \bar{d}(x, Q^2)$ , for different  $x$  and  $Q^2$  values.

Let us first consider the  $W$  production cross section which provides an important test of the quark densities determined from deep-inelastic scattering. For illustration we show in Fig.9 the rapidity distribution for  $\bar{p}p \rightarrow W^+ + X$  at Tevatron energy, which has been computed in the Drell-Yan picture, dominated by the product  $u(x, M_W^2)d(x, M_W^2)$  with  $x \sim 0.05$ . We find that the maximum value of  $d\sigma/dy_W$  is around  $2.6\text{nb}$  which is somehow smaller compared to other predictions presented in ref.[6]. For the total  $W$  cross section we find  $\sigma_W = 19\text{nb}$  which is compatible with recent experimental values from CDF and  $D_0$  at FNAL [29]. Next we turn to hadronic processes dominated by quark-antiquark annihilation, in order to study further the flavor symmetry breaking in the light sea quarks of the proton. One possibility, as noticed

in ref.[21], is to compare dilepton production in  $pp$  and  $pn$  collisions by means of the Drell-Yan asymmetry

$$A_{DY} = \frac{d\sigma_{pp}/dy - d\sigma_{pn}/dy}{d\sigma_{pp}/dy + d\sigma_{pn}/dy}. \quad (10)$$

These cross sections can be easily written in terms of  $q(x_a, M^2)$  and  $\bar{q}(x_b, M^2)$  and at rapidity  $y = 0$ , one has  $x_a = x_b = \sqrt{\tau} = M/\sqrt{s}$ , where  $M$  is the lepton pair mass. For the sake of simplicity, by neglecting the sea-sea contributions, one gets

$$A_{DY} = \frac{(4\lambda_v - 1)(\lambda_s - 1) + (\lambda_v - 1)(4\lambda_s - 1)}{(4\lambda_v + 1)(\lambda_s + 1) + (\lambda_v + 1)(4\lambda_s + 1)}, \quad (11)$$

where  $\lambda_v = u_{val}/d_{val}$  and  $\lambda_s = \bar{u}/\bar{d}$ . In a broad kinematical region where  $\lambda_v \sim 2$ , this expression shows the sensitivity of  $A_{DY}$  to  $\lambda_s$  and, for example, for a flavor symmetric sea i.e.  $\lambda_s = 1$ , one gets  $A_{DY} = 0.09$ , whereas  $\lambda_s = 0.5$  leads to  $A_{DY} = -0.09$ . This asymmetry has been measured at CERN by the NA51 Collaboration [22] in proton-proton and proton-deuteron collisions with  $450\text{GeV}/c$  incident protons, in the mass range  $4.3 < M < 8.5\text{GeV}$ . As shown in Fig.10, the asymmetry  $A_{DY}$  predicted by our parton densities is compatible with the result of this rather low statistics experiment. A more accurate determination of  $\lambda_s$  should be obtained in the near future at FNAL by the E866 experiment [23]. On the other hand, since there is a realistic possibility of having proton-proton and proton-deuteron collisions at RHIC with a high luminosity [24, 25], the measurement of  $A_{DY}$  should be seriously envisaged. In view of these future data, we give in Fig.11 the ratio  $(\bar{d} - \bar{u})/(\bar{d} + \bar{u})$  versus  $x$  for a standard lepton pair mass  $M = 5\text{GeV}$  (solid line).

A second possibility for testing the value of  $\lambda_s$  has been proposed in ref.[25] by means of the production of  $W^\pm$  and  $Z$  in  $pp$  and  $pn$  collisions, also accessible at RHIC which will have the required energy. For  $W^\pm$  production, let us consider the following ratio

$$R_W = \frac{d\sigma_{pp}^{W^+}/dy + d\sigma_{pp}^{W^-}/dy - d\sigma_{pn}^{W^+}/dy - d\sigma_{pn}^{W^-}/dy}{d\sigma_{pp}^{W^+}/dy + d\sigma_{pp}^{W^-}/dy + d\sigma_{pn}^{W^+}/dy + d\sigma_{pn}^{W^-}/dy}. \quad (12)$$

If we neglect the sea-sea contributions, it simply reads in terms of  $\lambda_v(x)$  and  $\lambda_s(x)$

$$R_W = -\frac{(\lambda_v(x_a) - 1)(\lambda_s(x_b) - 1) + (x_a \leftrightarrow x_b)}{(\lambda_v(x_a) + 1)(\lambda_s(x_b) + 1) + (x_a \leftrightarrow x_b)}. \quad (13)$$

Clearly  $R_W$  is symmetric under  $y \rightarrow -y$  and  $R_W = 0$  if the sea is flavor symmetric, i.e.  $\lambda_s(x) = 1$ . We show in Fig.12 our predictions for  $R_W$  at two different energies. We find that  $R_W$  is positive because  $\lambda_s$  is always less than one, as we can check from the dashed line in Fig.11 which corresponds to  $Q^2 = M_W^2$ .  $R_W$  decreases when  $\sqrt{s}$  increases because for smaller  $x$ , according to Fig.11,  $\lambda_s(x)$  increases and it follows from eq.(13) that  $R_W$  gets smaller. Actually the trend shown in Fig.11 is simply due to the fact that the difference  $\bar{d} - \bar{u}$  does not change with  $Q^2$ , whereas the sum  $\bar{d} + \bar{u}$  increases with increasing  $Q^2$ . The prediction obtained for  $R_W$  is slightly different from that of ref.[25] because we are now using a more reliable set of parton distributions.

## 4 Quark, antiquark, gluon helicity distributions and experimental tests

Since our approach is based on the direct construction of the quark (antiquark) parton distributions of a given helicity  $q_{val}^\pm$  and  $\bar{q}^\pm$ , we have nothing to add to the results of section 2 to obtain  $\Delta q_{val} = q_{val}^+ - q_{val}^-$  and  $\Delta \bar{q} = \bar{q}^+ - \bar{q}^-$  at  $Q^2 = Q_0^2$ . We recall the simple relations used in ref.[1] namely

$$x\Delta u_{val}(x, Q_0^2) = xu_{val}(x, Q_0^2) - xd_{val}(x, Q_0^2), \quad (14-a)$$

$$x\Delta d_{val}(x, Q_0^2) = -1/3xd_{val}(x, Q_0^2), \quad (14-b)$$

$$x\Delta \bar{u}(x, Q_0^2) = x\bar{u}(x, Q_0^2) - x\bar{d}(x, Q_0^2), \quad (14-c)$$

$$x\Delta \bar{d}(x, Q_0^2) = x\Delta s(x, Q_0^2) = x\Delta \bar{s}(x, Q_0^2) = 0. \quad (14-d)$$

We show in Fig.13 the different ratios  $\Delta q/q$  at  $Q^2 = 3GeV^2$  versus  $x$ . One finds the usual features for  $\Delta u/u$  (positive and growing at large  $x$ ) and for  $\Delta d/d$  (negative and growing at large  $x$ ), whereas  $\Delta \bar{u}/\bar{u}$  is very large and negative, which is less conventional, and  $\Delta \bar{d}/\bar{d}$  is zero. Concerning the helicity distribution of the gluon  $x\Delta G(x, Q_0^2)$ , in the absence of any serious experimental indication, we can only make some speculations. One possibility is what one can call the *soft gluon*, for which one assumes

$$x\Delta G(x, Q_0^2) = x^2G(x, Q_0^2) \quad (15-a)$$

and another one, is the *hard gluon*, where one takes

$$x\Delta G(x, Q_0^2) = \lambda(1-x)x^2G(x, Q_0^2) \quad (15-b)$$

with  $\lambda = 4$  which is the maximum value allowed to obey positivity, i.e.  $\Delta G < G$ . The integral of  $\Delta G(x)$  for the hard gluon case is about four times larger than for the soft gluon case. Note that for these two possibilities we assume  $\Delta G(x) > 0$ , which need not be true. In Fig.14, together with  $xG(x)$ , we show  $x\Delta G(x)$  for these two choices which do not involve any additional parameter.

Having fixed all these helicity distributions at  $Q^2 = Q_0^2$ , at higher  $Q^2$  they are obtained from the DGLAP evolution equations [5]. For the valence contributions, since the splitting functions are the same for  $q_{val}$  and  $\Delta q_{val}$ , one can evolve indifferently the r.h.s. or the l.h.s. of eqs.(14-a,14-b), it will lead to the same result which is, anyway, independent of the gluon helicity distribution. This is not the case for the antiquarks and in particular for  $\Delta\bar{u}$ , if one evolves the r.h.s. of eq.(14-c), the contribution coming from  $G(x, Q^2)$  will cancel in the difference. This situation corresponds to the assumption  $\Delta G(x, Q^2) \equiv 0$  for all  $Q^2$ . On the other hand, if one evolves correctly the l.h.s. of eq.(14-c), it will depend on  $\Delta G(x, Q^2)$  for which we can make either of the two different choices mentioned above. For the antiquarks, one can also assume that eq.(14-d) remains valid for all  $Q^2$  or starting from zero at  $Q^2 = Q_0^2$  one generates a non-zero  $\Delta\bar{q}$  at higher  $Q^2$  from the correct  $Q^2$  evolution with either the soft or the hard gluon. In Fig.15a,b we show the different ratios  $\Delta q/q$  versus  $x$  evaluated at  $Q^2 = M_W^2$  for the three different situations described above. For  $\Delta u/u$  the results are very similar and  $\Delta\bar{u}/\bar{u}$  decreases in magnitude for a harder gluon. This is also the case for  $\Delta d/d$ , but it is reversed for  $\Delta\bar{d}/\bar{d}$ . Finally we would like to recall that for the gluon helicity distribution, due to the QCD evolution, one obtains [26] in the very small  $x$  region

$$\Delta G(x, Q^2)/G(x, Q^2) \underset{x \rightarrow 0}{\sim} x \exp \left[ 0.8 \sqrt{S(Q^2) \ln 1/x} \right] \quad (16)$$

for six quark flavors, where  $S(Q^2) = \ln t/t_0$  and  $t = \ln Q^2/\Lambda^2$ , so at fixed  $x$  it grows for large  $Q^2$ .

We now turn to some of the predictions we can make from these distributions for helicity dependent observables. Let us start with the polarized structure functions for proton  $g_1^p(x, Q^2)$ , for neutron  $g_1^n(x, Q^2)$  and for deuteron  $g_1^d(x, Q^2)$ . In Fig.16 we have collected different sets of data for  $xg_1^p$ , the earlier EMC results [27] and the SMC results [28] corresponding to  $< Q^2 > = 10 GeV^2$  and the very recent E143 results [29] corresponding to

$\langle Q^2 \rangle = 3\text{GeV}^2$ . We also show for comparison our theoretical predictions, down to the lowest  $x$  range evaluated at these two  $Q^2$  values. The agreement is very satisfactory and gives strong support to our simple relations eqs.(14-a, 14-b, 14-c, 14-d) between unpolarized and polarized parton densities. For the integrals of  $g_1^p$  we find

$$\int_{0.003}^{0.7} g_1^p(x, Q^2) dx = 0.132 \quad \text{at} \quad Q^2 = 10\text{GeV}^2 \quad (17\text{-a})$$

compared to the SMC value [28]  $0.131 \pm 0.011 \pm 0.011$  and

$$\int_{0.029}^{0.8} g_1^p(x, Q^2) dx = 0.112 \quad \text{at} \quad Q^2 = 3\text{GeV}^2 \quad (17\text{-b})$$

compared to the E143 value [29]  $0.120 \pm 0.004 \pm 0.008$ . In both cases one finds results, at least two standard deviations, below the Ellis-Jaffe sum rule [30] with QCD corrections [31].

Concerning the neutron polarized structure function  $xg_1^n(x)$ , we show in Fig.17 a comparison of the E142 data [32] at  $Q^2 = 2\text{GeV}^2$  with our theoretical calculations. The dashed line corresponds to the case where one would assume that  $d$  quarks are not polarized, i.e.  $\Delta d(x) \equiv 0$ , and it clearly disagrees with the data. However by including the  $d$  valence quark polarization only according to eq.(14-b), we obtain the solid line in perfect agreement with the data and we find for  $Q^2 = 2\text{GeV}^2$

$$\int_0^1 g_1^n(x) dx = -0.020 . \quad (18)$$

Finally for the deuteron polarized structure function  $g_1^d$ , let us recall that we have the standard relation

$$g_1^d(x) = \frac{1}{2} (g_1^p(x) + g_1^n(x)) (1 - 1.5\omega_D) , \quad (19)$$

where  $\omega_D$  is the  $D$ -state probability in the deuteron. We show in Fig.18 our theoretical prediction at  $Q^2 = 3\text{GeV}^2$  compared to the preliminary E143 data [33] which are more accurate than the earlier SMC data [34]. For the integral in the  $x$  range covered by E143 we find

$$\int_{0.029}^{0.8} g_1^d(x) dx = 0.043 \quad (20)$$

in fair agreement with the experimental value [33]  $0.044 \pm 0.004 \pm 0.004$ .

Concerning the important issue of the validity of the Bjorken sum rule [35], our calculations at  $Q^2 = 5\text{GeV}^2$  leads to

$$\int_0^1 [g_1^p(x, Q^2) - g_1^n(x, Q^2)] dx = 0.158 \quad (21)$$

perfectly compatible with the best experimental estimate [28] that is  $0.166 \pm 0.017$ . However this is in slight disagreement with the present theoretical estimate, including QCD corrections [36] up to the third order in  $\alpha_s$ , which gives  $0.185 \pm 0.004$ . We recall that, to begin with, we did not impose this constraint on our distributions.

Before moving to hadronic collisions, we would like to close this discussion with a few words on the "transverse" spin dependent structure function  $g_2(x, Q^2)$  which can be measured in polarized deep-inelastic scattering with a transversely polarized target. The properties of  $g_2$  have been reviewed recently together with some estimates [37] and we recall that  $g_2$  can be thought as a sum of two terms

$$g_2(x, Q^2) = g_2^{WW}(x, Q^2) + \bar{g}_2(x, Q^2) , \quad (22)$$

where the first term is a twist-2 contribution [38] determined entirely by  $g_1(x, Q^2)$  since we have

$$g_2^{WW}(x, Q^2) = -g_1(x, Q^2) + \int_x^1 \frac{dy}{y} g_1(y, Q^2) \quad (23)$$

The second term in eq.(22) has twist-3 contributions, determined by quark-gluon interactions, and has a priori, no reason to be small. Given our present knowledge on  $g_1$ , we can use eq.(23) to evaluate  $g_2^{WW}$ . This is shown in Fig.19 for the proton case and a comparison with future experimental results will provide an estimate of  $\bar{g}_2$ .

Next we propose some tests using hadronic collisions, in particular in the framework of the future spin physics programme at RHIC which is planned to be used as a polarized  $pp$  collider [24]. Many helicity dependent observables have been calculated in ref.[25] and our purpose here is just to show how to update our earlier predictions, using this new set of helicity distributions. Let us first consider the parity-violating helicity asymmetry  $A_L$  defined as

$$A_L = \frac{d\sigma_-/dy - d\sigma_+/dy}{d\sigma_-/dy + d\sigma_+/dy} \quad (24)$$

In  $W^+$  production, it reads

$$A_L(y) = \frac{\Delta u(x_a, M_W^2)\bar{d}(x_b, M_W^2) - (u \leftrightarrow \bar{d})}{u(x_a, M_W^2)\bar{d}(x_b, M_W^2) + (u \leftrightarrow \bar{d})}, \quad (25)$$

assuming the proton  $a$  is polarized. For  $W^-$  production, the quark flavors are interchanged. Using our set of polarized quark densities, we find at  $\sqrt{s} = 500\text{GeV}$ , the predictions shown in Fig.20. Near  $y = +1$ ,  $A_L^{W^+} \sim \Delta u/u$  and  $A_L^{W^-} \sim \Delta d/d$  evaluated at  $x = 0.435$ , whereas near  $y = -1$   $A_L^{W^+} \sim -\Delta\bar{d}/\bar{d}$  and  $A_L^{W^-} \sim -\Delta\bar{u}/\bar{u}$  evaluated at  $x = 0.059$ . Therefore the trends in Fig.20 can be easily compared with the shapes displayed in Figs.15a,b which also show the sensitivity to the choice of either soft gluon or hard gluon helicity distribution.

In  $pp$  collisions where both proton beams are polarized, there is another observable which is very sensitive to antiquark polarizations, that is the parity-conserving double helicity asymmetry  $A_{LL}$  defined as

$$A_{LL} = \frac{d\sigma_{++}/dy + d\sigma_{--}/dy - d\sigma_{+-}/dy - d\sigma_{-+}/dy}{d\sigma_{++}/dy + d\sigma_{--}/dy + d\sigma_{+-}/dy + d\sigma_{-+}/dy}. \quad (26)$$

In lepton-pair production, it reads

$$A_{LL} = -\frac{\sum_i e_i^2 [\Delta q_i(x_a)\Delta\bar{q}_i(x_b) + (x_a \leftrightarrow x_b)]}{\sum_i e_i^2 [q_i(x_a)\bar{q}_i(x_b) + (x_a \leftrightarrow x_b)]}, \quad (27)$$

where  $e_i$  is the electric charge of the quark  $q_i$ .

We have calculated  $A_{LL}$  at  $\sqrt{s} = 100\text{GeV}$  which seems best appropriate to the acceptance of the detectors at RHIC and the results, in the soft gluon case, are shown in Fig.21. We observe that  $A_{LL}$  is positive because it is dominated by  $\Delta u\Delta\bar{u}$ , where  $\Delta\bar{u}$  is negative.  $A_{LL}$  increases with increasing lepton-pair  $M$  and of course for  $\Delta\bar{u} = \Delta\bar{d} = 0$  we would have  $A_{LL} = 0$ . Obviously these tests can be extended by many other examples as shown in ref.[25], in particular parity-violating and parity-conserving helicity asymmetries in  $W^\pm$ ,  $Z$  production in  $pp$  and  $pn$  collisions.

## 5 Double spin transverse asymmetries $A_{TT}$

So far we have considered collisions involving only longitudinally polarized proton beams, but of course at RHIC, transversely polarized protons will

be available as well [24]. This new possibility is extremely appealing because of recent progress in understanding transverse spin effects in QCD, both at leading twist [39] and higher twist levels [40]. For the case of the nucleon's helicity, its distribution among the various quarks and antiquarks can be obtained in polarized deep-inelastic scattering from the measurement of the structure function  $g_1(x)$  mentioned above. However this is not possible for the *transversity* distribution  $h_1(x)$  which describes the state of a quark (antiquark) in a transversely polarized nucleon. The reason is that  $h_1(x)$ , which measures the correlation between right-handed and left-handed quarks, decouples from deep-inelastic scattering. Indeed like  $g_1(x)$ ,  $h_1(x)$  is leading - twist and it can be measured in Drell-Yan lepton-pair production with both initial proton beams transversely polarized [39]. Other possibilities have been suggested [41] but in the framework of this paper, we will envisage also a practical way to determine  $h_1(x)$ , by using gauge boson production in  $pp$  collisions with protons transversely polarized. Let us consider the double spin transverse asymmetry defined as

$$A_{TT} = \frac{\sigma_{\uparrow\uparrow} - \sigma_{\uparrow\downarrow}}{\sigma_{\uparrow\uparrow} + \sigma_{\uparrow\downarrow}} \quad (28)$$

where  $\sigma_{\uparrow\uparrow}(\sigma_{\uparrow\downarrow})$  denotes the cross section with the two initial protons transversely polarized in the same (opposite) direction. Assuming that the underlying parton subprocess is quark-antiquark annihilation, we easily find for  $Z$  production

$$A_{TT} = \frac{\sum_{i=u,d} (b_i^2 - a_i^2) [h_1^{q_i}(x_a) h_1^{\bar{q}_i}(x_b) + (x_a \leftrightarrow x_b)]}{\sum_{i=u,d} (a_i^2 + b_i^2) [q_i(x_a) \bar{q}_i(x_b) + (x_a \leftrightarrow x_b)]}. \quad (29)$$

This result generalizes the case of the lepton-pair production [39] through an off-shell photon  $\gamma^*$  corresponding to  $b_i = 0$  and  $a_i = e_i$  and which gives

$$A_{TT} = a_{TT} \frac{\sum_i e_i^2 [h_1^{q_i}(x_a) h_1^{\bar{q}_i}(x_b) + (x_a \leftrightarrow x_b)]}{\sum_i e_i^2 [q_i(x_a) \bar{q}_i(x_b) + (x_a \leftrightarrow x_b)]}, \quad (30)$$

where  $a_{TT}$  is the parton asymmetry which has a simple expression in the c.m. frame of the lepton-pair [39].

For  $W^\pm$  production, which is pure left-handed and therefore does not allow right-left interference, we expect  $A_{TT} = 0$ , since in this case  $a_i^2 = b_i^2$ . This result is worth checking experimentally.

So far there is no experimental data on these distributions  $h_1^q(x)$  (or  $h_1^{\bar{q}}(x)$ ), but there are some attempts to calculate them either in the framework of the MIT bag model [39] or by means of QCD sum rules [42]. However the use of positivity yields to derive a model-independent constraint on  $h_1^q(x)$  which restricts substantially the domain of allowed values [43]. Indeed one has obtained

$$q(x) + \Delta q(x) \geq 2|h_1^q(x)| . \quad (31)$$

which is much less trivial than

$$q(x) \geq |h_1^q(x)| , \quad (32)$$

as proposed earlier in ref. [39].

In the MIT bag model, let us recall that these distributions read [39]

$$q = f^2 + g^2, \quad \Delta q = f^2 - 1/3g^2 \quad \text{and} \quad h_1^q = f^2 + 1/3g^2 \quad (33)$$

and they saturate eq.(31). In this case, we observe that  $h_1^q(x) \geq \Delta q(x)$  but this situation cannot be very general because of eq.(31). As an example let us assume  $h_1^q(x) = 2\Delta q(x)$ . Such a relation cannot hold for all  $x$  and we see that eq.(31), in particular if  $\Delta q(x) > 0$ , implies  $q(x) \geq 3\Delta q(x)$ . This is certainly not satisfied for all  $x$  by the present determination of the  $u$  quark helicity distribution, in particular for large  $x$  where  $A_1^p(x)$  is large [27, 28, 29]. The simplifying assumption  $h_1^q(x) = \Delta q(x)$ , based on the non-relativistic quark model, which has been used in some recent calculations [25, 41] is also not acceptable for all  $x$  values if  $\Delta q(x) < 0$  because of eq.(31). To illustrate the practical use of eq.(31), let us consider eqs.(14-a) and (14-c). It is then possible to obtain the allowed range of values for  $h_1^u(x)$ , namely

$$u(x) - \frac{1}{2}d(x) \geq |h_1^u(x)| \quad (34)$$

and similarly for  $\bar{u}$ .

We now turn to some predictions for  $A_{TT}$  which will depend heavily on our assumptions. Since the  $u$  quark term is expected to dominate because of the charge factor, we assume  $h_1^{\bar{d}} = 0$  and we take the equality sign in eq.(34) assuming  $h_1^u(x) > 0$  and  $h_1^{\bar{u}}(x) < 0$ . We show in Figs.22a,b our results for  $A_{TT}/a_{TT}$  in dilepton production at two energies  $\sqrt{s} = 50$  and  $100\text{GeV}$  for several values of the dilepton mass  $M$ . The effect is larger for increasing  $M$

because at fixed energy it corresponds to higher  $x$  values where  $\Delta u$  and  $\Delta \bar{u}$  are larger, as well as  $h_1^u$  and  $h_1^{\bar{u}}$ . Of course, at fixed  $M$  the effect decreases with increasing energy. Finally we show in Fig.23 our predictions for  $A_{TT}$  in  $Z$  production at two different energies  $\sqrt{s} = 350$  and  $500\text{GeV}$ . Clearly these predictions are only a guide for future experiments at RHIC which will indeed lead to the actual determination of  $h_1(x)$ .

## 6 Concluding remarks

We have presented a new set of quark-parton densities in terms of Fermi-Dirac distributions depending on *nine* free parameters which were determined from the spin-average structure functions at low  $Q^2$ . Some simple relations between unpolarized and polarized densities, which were postulated earlier, are well supported by recent data on spin-dependent structure functions. We have also proposed a simple expression for the gluon density in terms of a Bose-Einstein distribution with no additional free parameter. We have then used a straightforward DGLAP  $Q^2$  evolution to get access to a broad  $x$  and  $Q^2$  range in order to test our approach with a large number of deep-inelastic scattering data. The predictions give a very satisfactory description of the CCFR, NMC, BCDMS, SLAC data and we also get, in a natural way, the sharp rise of  $F_2^{ep}(x, Q^2)$  for small  $x$ , recently observed at HERA by the H1 and Zeus Collaborations. So this is a brilliant confirmation of the validity of perturbative QCD, to be confronted to more accurate future data at HERA. We have also discussed the relevant question of flavor symmetry breaking of the light sea quarks (or antiquarks) of the nucleon which has to be measured in a broader  $x$  and  $Q^2$  range. To extend the polarized antiquark (or sea quark) parton densities to large  $Q^2$ , we have to make a choice for the polarized gluon distribution and we used two possibilities, the soft gluon and the hard gluon. None of these is favoured at present and experiment will have to decide. Predictions were given for future measurements in hadronic collisions with longitudinally and transversely polarized proton beams at RHIC which will allow further tests of our approach in the spin sector, in particular for dilepton and  $W^\pm, Z$  production.

## Acknowledgments

We are grateful to G. Altarelli, B. Badelek, J. Feltesse, E. Hughes, J. Kwiecinski, J.F. Laporte, R. Roberts, W. Stirling, Y. Terrien, M. Virchaux and R. Windmolders for providing useful informations and for helpful discussions.

## References

- [1] C. BOURRELY and J. SOFFER, preprint CPT-94/P.3032, to be published in Phys. Rev. D.
- [2] P.Z. QUINTAS et al., (CCFR Collaboration), Phys. Rev. Lett. **71** (1993) 1307 ; W.C. LEUNG et al., (CCFR Collaboration), Phys. Lett. **B317** (1993) 655.
- [3] C. FODAS et al., Phys. Rev. Lett. **64** (1990) 1207 ; S.R. MISHRA et al., Phys. Rev. Lett. **68** (1992) 3499 ; S.A. RABINOWITZ et al., Phys. Rev. Lett. **70** (1993) 134.
- [4] M. ARNEODO et al., (New Muon Collaboration), Phys. Rev. **D50** (1994) R1 and references therein.
- [5] V.N. GRIBOV and L.N. LIPATOV, Sov. J. Nucl. Phys. **15** (1972) 438, 675 ; G. ALTARELLI and G. PARISI, Nucl. Phys. **B126** (1977) 298 ; Yu.L. DOKSHITZER, Sov. J. JETP **46** (1977) 641.
- [6] A.D. MARTIN, R.G. ROBERTS and W.J. STIRLING, Phys. Rev. **D50** (1994) 6734 and references therein.
- [7] J. BOTTS et al., (CTEQ Collaboration), Phys. Lett. **B304** (1993) 159.
- [8] T. GEHRMANN and W.J. STIRLING, preprint DTP/94/38, may 1994.
- [9] J. KWIECINSKI and D. STROZIK-KOTLORZ, Z. Phys. **C48** (1990) 315.
- [10] P. AMAUDRUZ et al., (New Muon Collaboration), Phys. Lett. **B295** (1992) 159.

- [11] A.C. BENVENUTI et al., (BCDMS Collaboration), Phys. Lett. **B223** (1989) 485 ; and **B237** (1990) 592.
- [12] M. DERRICK et al., (Zeus Collaboration), preprint DESY-94-143, august 1993, submitted to Z. Phys. C.
- [13] T. AHMED et al., (H1 Collaboration), preprint DESY-95-006, January 1995.
- [14] M. DERRICK et al., (Zeus Collaboration), preprint DESY-94-176, October 1993, submitted to Z. Phys. C.
- [15] L. WHITLOW et al., Phys. Lett. **B282** (1992) 475.
- [16] A.V. KOTVAL et al., (E665 Collaboration) presented at the VI<sup>th</sup> Rencontre de Blois, France, June 1994.
- [17] For a nice review see, B. BABELEK and J. KWIECINSKI, preprint Warsaw University IFD/1/1994, August 1994.
- [18] G. PREPARATA, P.G. RATCLIFFE and J. SOFFER, Phys. Rev. Lett. **66** (1991) 687.
- [19] P. AMAUDRUZ et al., (New Muon Collaboration), Phys. Rev. Lett. **66** (1991) 2712.
- [20] F. ABE et al., (CDF Collaboration), Phys. Rev. Lett. **69** (1992) 28 ; P. GRUDBERG and C. GERBER (D<sub>0</sub> Collaboration), presented at the Meeting of the APS, Washington DC, April (1994).
- [21] S.D. ELLIS and W.J. STIRLING, Phys. Lett. **B256** (1991) 258.
- [22] A. BALDIT et al., (NA51 Collaboration), Phys. Lett. **B332** (1994) 244.
- [23] G.T. GARVEY, Fermilab E 866 experiment, Spokesman.
- [24] G. BUNCE et al., (RSC Collaboration), Particle World **3** (1992) 1 ; Proposal on Spin Physics using the RHIC Polarized Collider, R5 (14 August 1992), approved October 1993.
- [25] C. BOURRELY and J. SOFFER, Nucl. Phys. **B423** (1994) 329.

- [26] M.B. EINHORN and J. SOFFER, Nucl. Phys. **B274** (1986) 714.
- [27] J. ASHMAN et al., (European Muon Collaboration), Phys. Lett. **B206** (1988) 364 ; Nucl. Phys. **B328** (1989) 1.
- [28] D. ADAMS et al., (Spin Muon Collaboration), Phys. Lett. **B329** (1994) 399.
- [29] K. ABE et al., (E 143 Collaboration), Phys. Rev. Lett. **74** (1995) 346.
- [30] J. ELLIS and R. JAFFE, Phys. Rev. **D9** (1974) 1444.
- [31] S.A. LARIN, Phys. Lett. **B334** (1994) 192.
- [32] P.L. ANTHONY et al., (E 142 Collaboration), Phys. Rev. Lett. **71** (1993) 959.
- [33] Y. TERRIEN, Talk presented at the XII International Seminar on High Energy Physics Problems Relativistic Nuclear Physics & Quantum Chromodynamics, Dubna, September 1994, preprint DAPNIA/SPhN-9452.
- [34] B. ADEVA et al., (Spin Muon Collaboration), Phys. Lett. **B302** (1993) 533.
- [35] J.D. BJORKEN, Phys. Rev. **148** (1966) 1467 ; Phys. Rev. **D1** (1970) 1376.
- [36] S.A. LARIN and J.A.M. VERMASEREN, Phys. Lett. **B259** (1991) 345.
- [37] R. JAFFE, Comm. Nucl. Part. Phys. **14** (1990) 239 ; R. JAFFE and X. JI, Phys. Rev. **D43** (1991) 724.
- [38] S. WANDZURA and F. WILCZEK, Phys. Lett. **72B** (1977) 195.
- [39] J. RALSTON and D.E. SOPER, Nucl. Phys. **B152** (1979) 109 ; J.L. CORTES, B. PIRE and J. RALSTON, Z. Phys. **C55** (1992) 409 ; R. JAFFE and X. JI, Phys. Rev. Lett. **67** (1991) 552 ; R. JAFFE and X. JI, Nucl. Phys. **B375** (1992) 527 ; X. JI, Nucl. Phys. **B402** (1993) 217.

- [40] J. QIU and G. STERMAN, Nucl. Phys. **B378** (1992) 52 ; R. JAFFE and X. JI, Phys. Rev. **D43** (1991) 724.
- [41] X. JI, Phys. Lett. **B234** (1992) 137 ; R. JAFFE and X. JI, Phys. Rev. Lett. **71** (1993) 2547.
- [42] B.L. IOFFE and A. KHODJAMARIAN, preprint University of München LMU-01-94.
- [43] J. SOFFER, preprint CPT-94/P.3059, To be published Phys. Rev. Lett.

## Figure Captions

- Fig.1a The structure function  $x F_3^{\nu N}(x, Q^2)$  versus  $x$ . Data are from ref.[2] at  $Q^2 = 3 GeV^2$ , the solid line is the result of our fit and the dashed curve represents the MRS (A) parametrization at  $Q^2 = 4 GeV^2$  from ref.[6].
- Fig.1b The antiquark contribution  $x \bar{q}(x) = x \bar{u}(x) + x \bar{d}(x) + x \bar{s}(x)$  at  $Q^2 = 3 GeV^2$  (full circles) and  $Q^2 = 5 GeV^2$  (full triangles) versus  $x$ . Data are from ref.[3], the solid line is the result of our fit and the dashed curve represents the MRS (A) parametrization at  $Q^2 = 4 GeV^2$  from ref.[6].
- Fig.2a The difference  $F_2^p(x) - F_2^n(x)$  at  $Q^2 = 4 GeV^2$  versus  $x$ . Data are from ref.[4], the solid line is the result of our calculation and the dashed curve represents the MRS (A) parametrization at  $Q^2 = 4 GeV^2$  from ref.[6].
- Fig.2b The ratio  $F_2^n(x)/F_2^p(x)$  at  $Q^2 = 4 GeV^2$  versus  $x$ . Data are from ref.[4], the solid line is the result of our calculation and the dashed curve represents the MRS (A) parametrization at  $Q^2 = 4 GeV^2$  from ref.[6].
- Fig.3 The unpolarized parton distributions as a function of  $x$  at two different  $Q^2$  values,  $Q^2 = 3 GeV^2$  (solid lines) and  $Q^2 = 20 GeV^2$  (dashed lines).
- Fig.4 The gluon density  $x G(x, Q^2)$  versus  $x$  at two different  $Q^2$  values,  $Q^2 = 3 GeV^2$  (solid line) and  $Q^2 = 20 GeV^2$  (dashed line).

- Fig.5 The description of the CCFR data [2] of the  $x F_3^{\nu N}(x, Q^2)$  structure function, given by our parton densities. The theoretical curves are shown after an overall renormalization by a factor 1.04.
- Fig.6a The description of the NMC data [10] (full circles) and BCDMS data [11] (open circles) of the  $F_2^{\mu p}(x, Q^2)$  structure function given by our parton densities versus  $Q^2$  for  $x$  bins between  $x = 0.0125$  and  $x = 0.14$ . The theoretical curves are shown after an overall renormalization by a factor 1.12.
- Fig.6b Same as Fig.6a for  $x$  bins between  $x = 0.18$  and  $x = 0.75$ .
- Fig.7a The description of the Zeus data [12] (full triangles) and H1 data [13] (full circles) of the  $F_2^{ep}(x, Q^2)$  structure function given by our parton densities versus  $x$  for  $Q^2$  bins between  $Q^2 = 4.5 GeV^2$  and  $Q^2 = 25 GeV^2$ .
- Fig.7b Same as Fig.7a for  $Q^2$  bins between  $Q^2 = 35 GeV^2$  and  $200 GeV^2$ .
- Fig.7c Same as Fig.7a for  $Q^2$  bins between  $Q^2 = 250 GeV^2$  and  $5000 GeV^2$ .
- Fig.8a The description of the NMC data [10] (full circles) and SLAC data [15] (open circles) of the  $F_2^{\mu p}(x, Q^2)$  structure function in the low  $Q^2$ , low  $x$  region given by our parton densities for  $x$  bins between  $x = 0.00375$  and  $x = 0.0175$ . The theoretical curves are shown after an overall renormalization by a factor 1.12.
- Fig.8b Same as Fig.8a for  $x$  bins between  $x = 0.025$  and  $x = 0.14$ .
- Fig.9 The  $W^+$  rapidity distribution in  $\bar{p}p$  collisions at  $\sqrt{s} = 1.8 TeV$  predicted by our parton densities.
- Fig.10 Our theoretical prediction for  $A_{DY}$  (see eq.(10)) versus  $\sqrt{\tau} = M/\sqrt{s}$  compared to the NA51 data [22].
- Fig.11 Our predicted ratio  $(\bar{d} - \bar{u})/(\bar{d} + \bar{u})$  versus  $x$  for two different  $Q^2$  values ; solid line  $Q^2 = 25 GeV^2$  and dashed line  $Q^2 = M_W^2$ .
- Fig.12 The ratio  $R_W$  (see eq.(12)) versus  $y$  at  $\sqrt{s} = 250$  and  $350 GeV$ .
- Fig.13 The ratios  $\Delta u/u$ ,  $\Delta d/d$ ,  $\Delta \bar{u}/\bar{u}$  and  $\Delta \bar{d}/\bar{d}$  versus  $x$  at  $Q^2 = 3 GeV^2$ .

- Fig.14 The helicity gluon distribution  $x\Delta G(x)$  (soft gluon, dashed line and hard gluon, dotted line) versus  $x$  at  $Q^2 = 3GeV^2$  and for comparison the unpolarized gluon distribution  $xG(x)$  (solid line).
- Fig.15a The predicted ratios  $\Delta u/u$  and  $\Delta \bar{u}/\bar{u}$  versus  $x$  at  $Q^2 = M_W^2$ . The three curves correspond to the three cases for  $\Delta G$ : identically zero (solid line), soft gluon (eq.(15-a)) (dashed-dotted line) and hard gluon (eq.(15-b)) (dashed line).
- Fig.15b Same as Fig.15a for  $\Delta d/d$  and  $\Delta \bar{d}/\bar{d}$ .
- Fig.16  $xg_1^p(x)$  versus  $x$  at  $\langle Q^2 \rangle = 3GeV^2$  and  $10GeV^2$ . Data are from ref.[27] (full squares), ref.[28] (full circles) and ref.[29] (open circles). The curves are theoretical predictions at  $Q^2 = 3GeV^2$  (dashed line) and  $Q^2 = 10GeV^2$  (solid line).
- Fig.17  $xg_1^n(x)$  versus  $x$  at  $\langle Q^2 \rangle = 2GeV^2$ . Data are from ref.[32] together with our theoretical predictions (dashed line is the contribution of  $\Delta u(x)$  and  $\Delta \bar{u}(x)$  only and solid line is the contribution of  $\Delta u(x)$ ,  $\Delta \bar{u}(x)$  and  $\Delta d_{val}(x)$ ).
- Fig.18  $xg_1^d(x)$  versus  $x$  at  $\langle Q^2 \rangle = 3GeV^2$ . Preliminary data are from ref.[33] together with our theoretical prediction.
- Fig.19 Our theoretical prediction for  $g_2(x, Q^2)$  at  $Q^2 = 3GeV^2$  for proton target assuming  $\bar{g}_2 = 0$  (see eq.(22)).
- Fig.20 Parity-violating helicity asymmetry  $A_L$  versus  $y$  for  $W^\pm$  production in  $pp$  collisions at  $\sqrt{s} = 500GeV$ . Solid lines correspond to soft gluon and dashed lines to hard gluon.
- Fig.21 Parity-conserving helicity asymmetry  $A_{LL}$  versus  $y$  for dilepton production at  $\sqrt{s} = 100GeV$  and different values of the lepton-pair mass. The curves correspond to the soft gluon case.
- Fig.22a Predictions for  $A_{TT}/a_{TT}$  in dilepton production versus  $y$  for  $\sqrt{s} = 50GeV$  and  $M = 5, 10, 15GeV$ . The curves correspond to the soft gluon case.
- Fig.22b Same as Fig.22a for  $\sqrt{s} = 100GeV$ .
- Fig.23 Predictions for  $A_{TT}$  in  $Z$  production versus  $y$  for  $\sqrt{s} = 350$  and  $500GeV$ . The curves correspond to the soft gluon case.

This figure "fig1-1.png" is available in "png" format from:

<http://arxiv.org/ps/hep-ph/9502261v1>

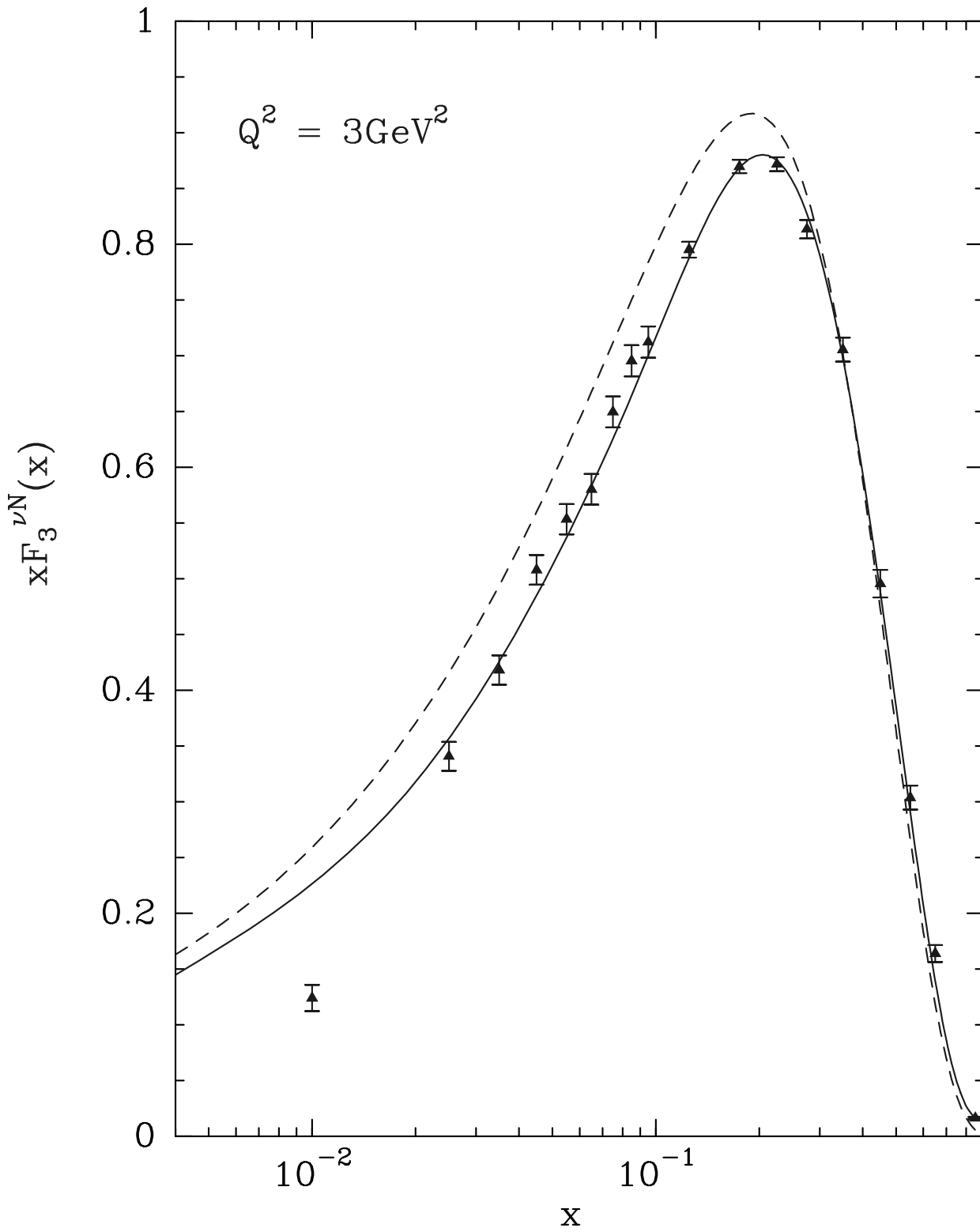


Fig 1a

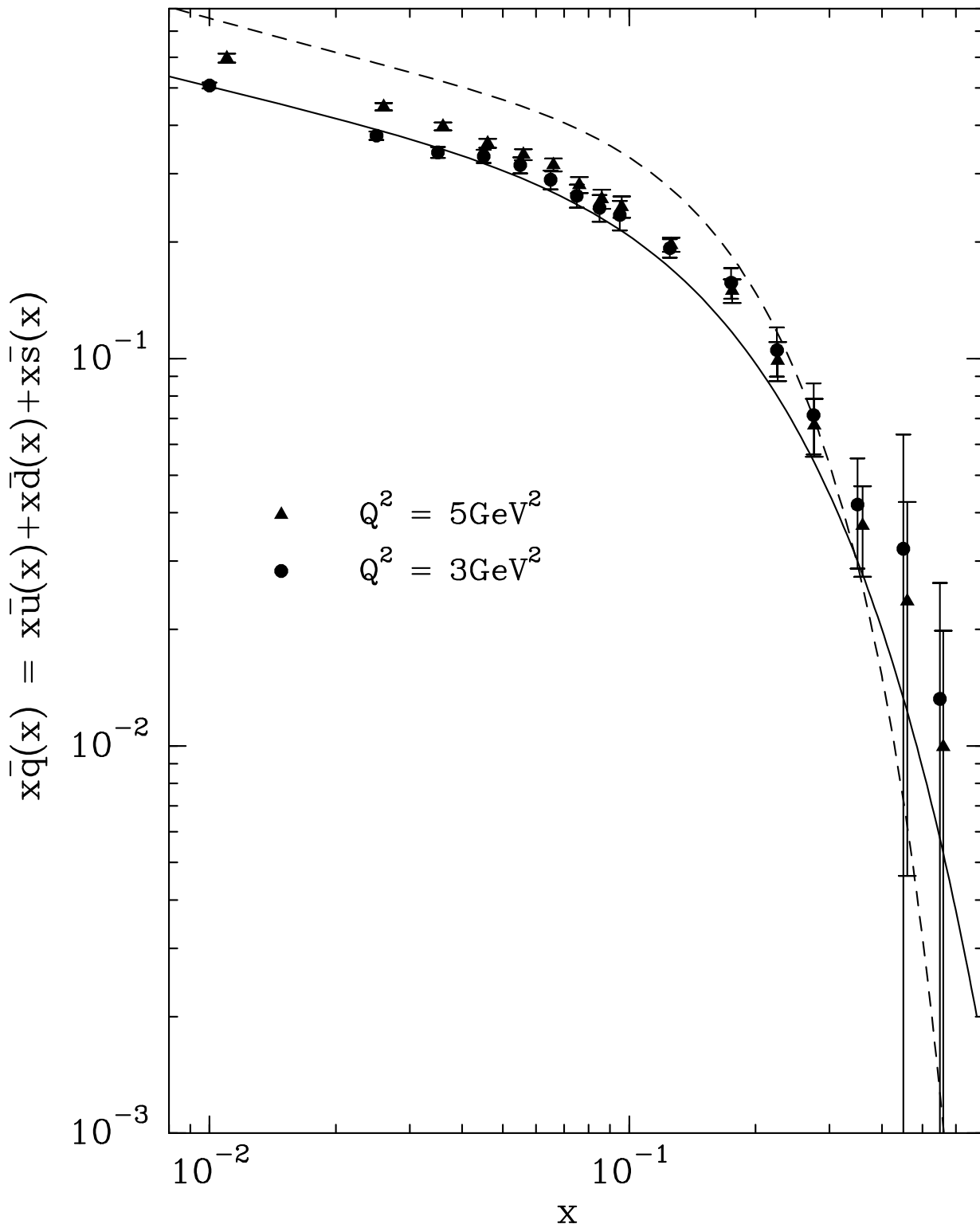


Fig 1b

This figure "fig2-1.png" is available in "png" format from:

<http://arxiv.org/ps/hep-ph/9502261v1>

This figure "fig3-1.png" is available in "png" format from:

<http://arxiv.org/ps/hep-ph/9502261v1>

This figure "fig4-1.png" is available in "png" format from:

<http://arxiv.org/ps/hep-ph/9502261v1>

This figure "fig1-2.png" is available in "png" format from:

<http://arxiv.org/ps/hep-ph/9502261v1>

This figure "fig2-2.png" is available in "png" format from:

<http://arxiv.org/ps/hep-ph/9502261v1>

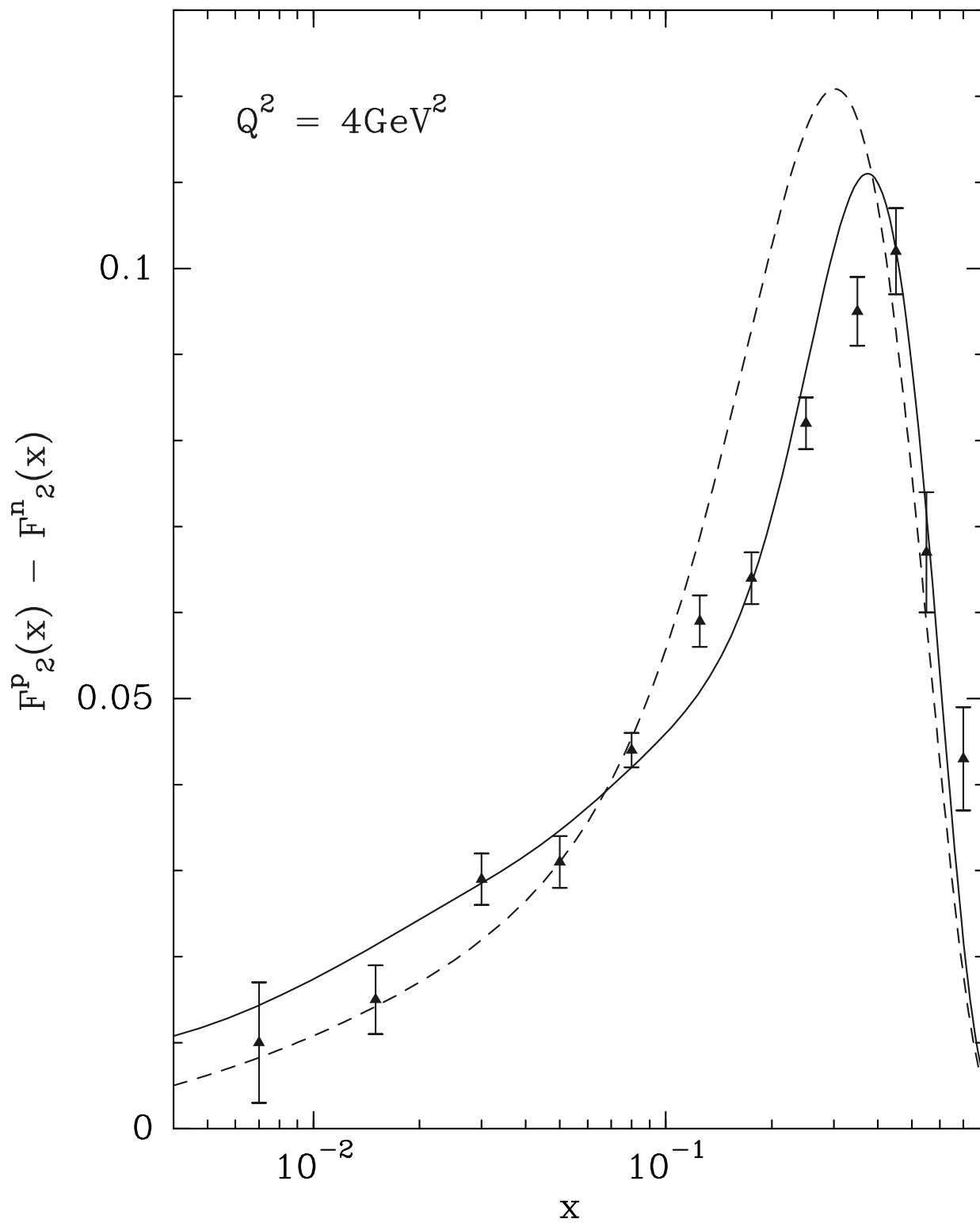


Fig 2a

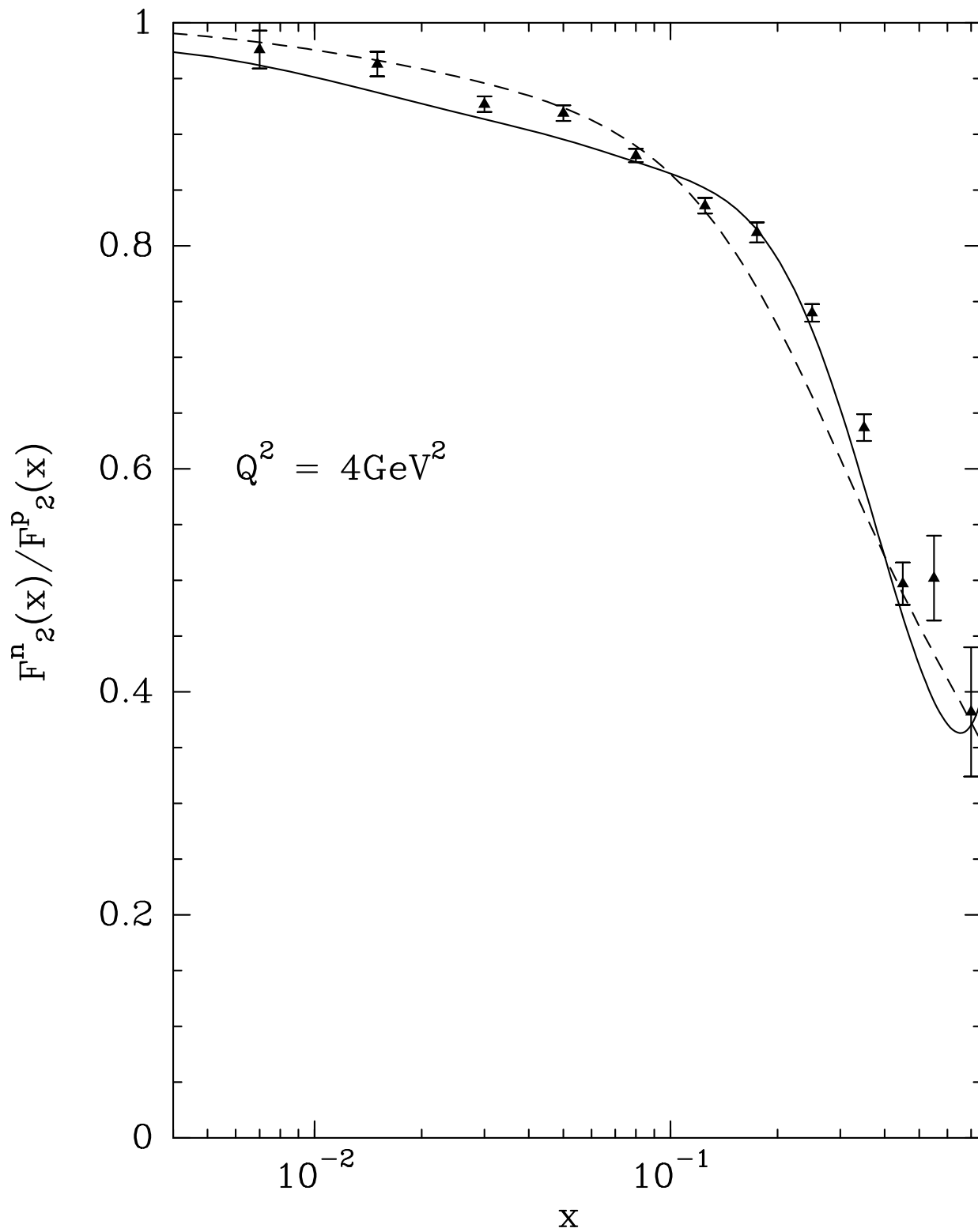


Fig 2b

This figure "fig3-2.png" is available in "png" format from:

<http://arxiv.org/ps/hep-ph/9502261v1>

This figure "fig4-2.png" is available in "png" format from:

<http://arxiv.org/ps/hep-ph/9502261v1>

This figure "fig1-3.png" is available in "png" format from:

<http://arxiv.org/ps/hep-ph/9502261v1>

This figure "fig2-3.png" is available in "png" format from:

<http://arxiv.org/ps/hep-ph/9502261v1>

This figure "fig3-3.png" is available in "png" format from:

<http://arxiv.org/ps/hep-ph/9502261v1>

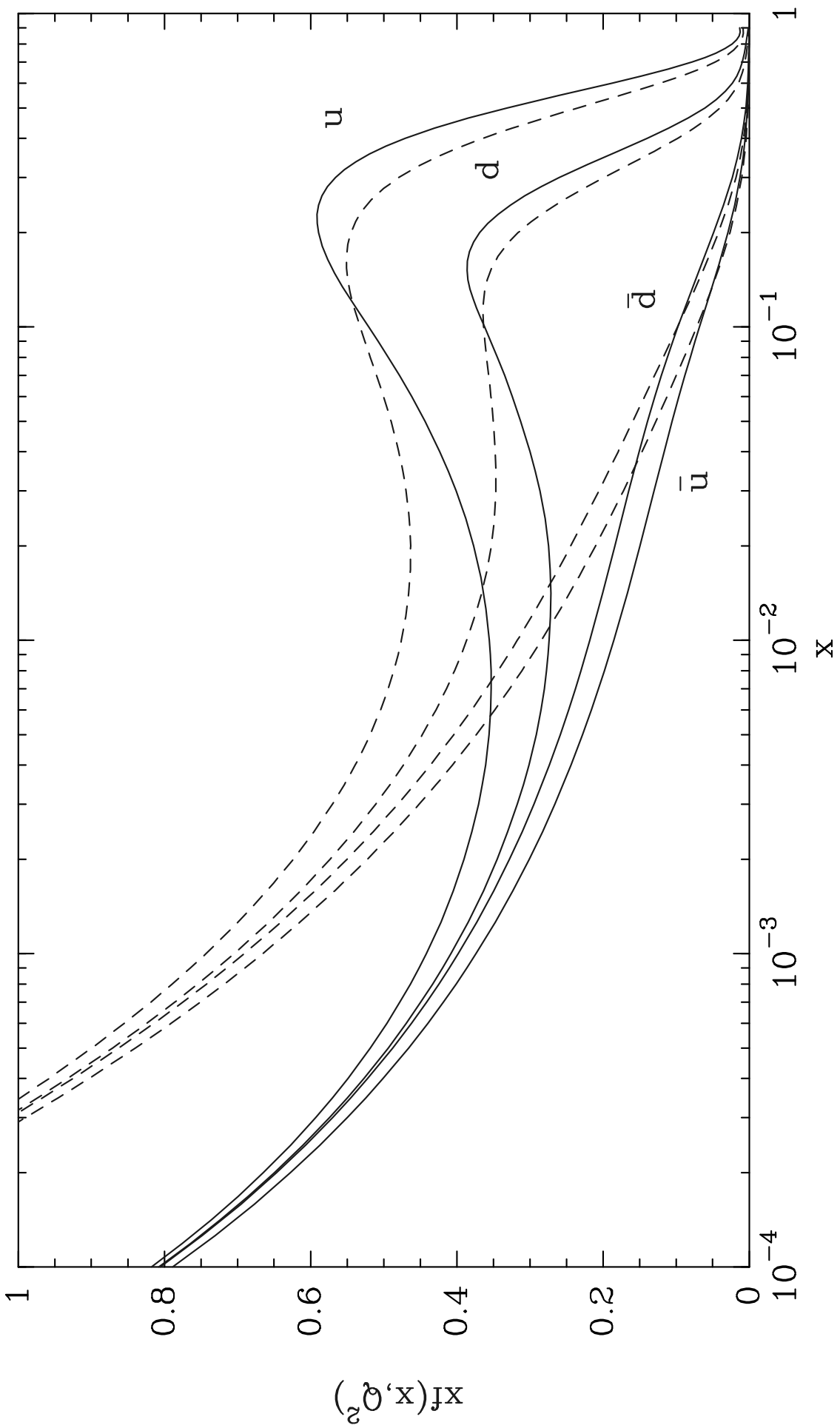


Fig 3

This figure "fig4-3.png" is available in "png" format from:

<http://arxiv.org/ps/hep-ph/9502261v1>

This figure "fig1-4.png" is available in "png" format from:

<http://arxiv.org/ps/hep-ph/9502261v1>

This figure "fig2-4.png" is available in "png" format from:

<http://arxiv.org/ps/hep-ph/9502261v1>

This figure "fig3-4.png" is available in "png" format from:

<http://arxiv.org/ps/hep-ph/9502261v1>

This figure "fig4-4.png" is available in "png" format from:

<http://arxiv.org/ps/hep-ph/9502261v1>

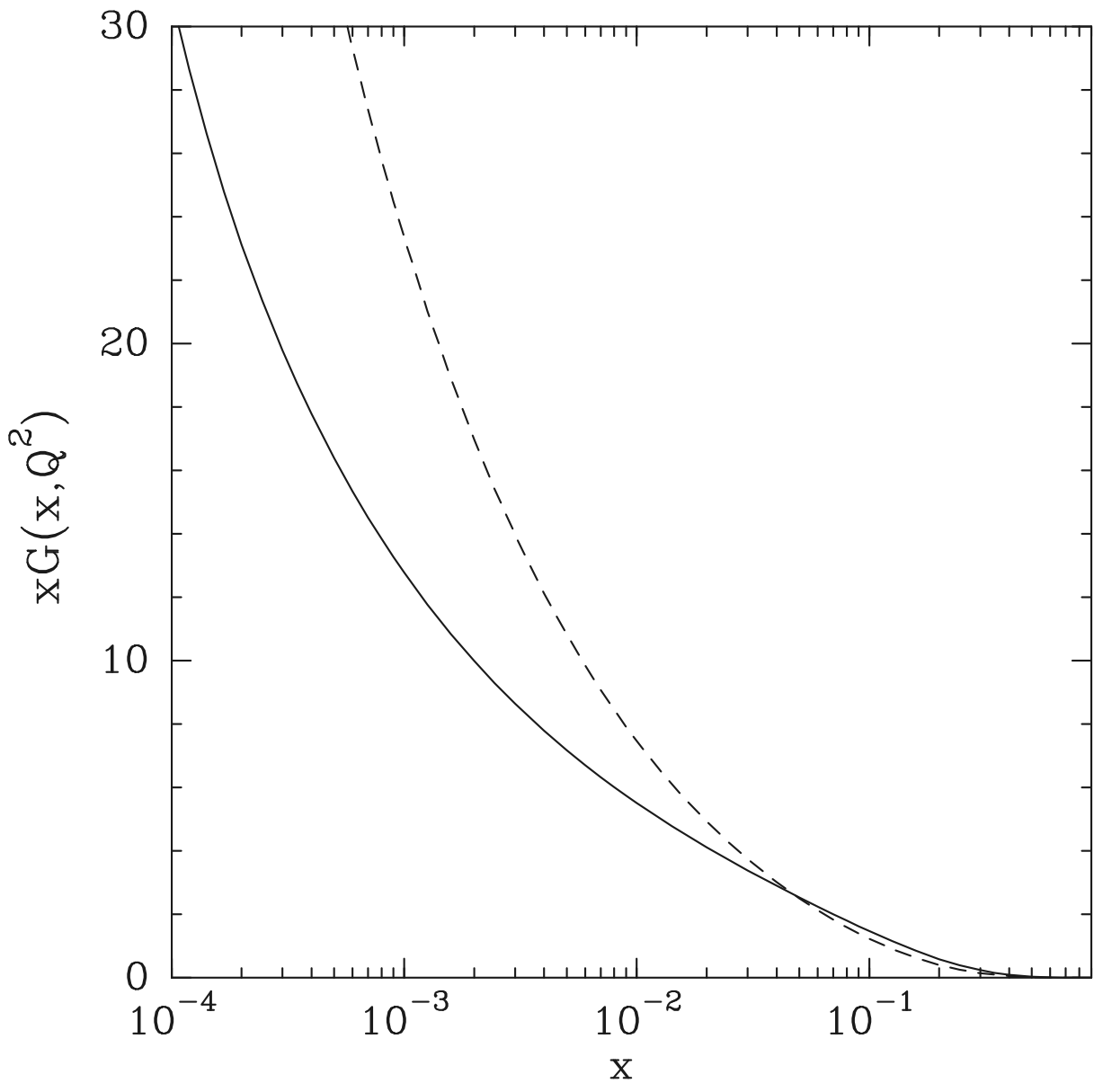


Fig 4

This figure "fig1-5.png" is available in "png" format from:

<http://arxiv.org/ps/hep-ph/9502261v1>

This figure "fig2-5.png" is available in "png" format from:

<http://arxiv.org/ps/hep-ph/9502261v1>

This figure "fig3-5.png" is available in "png" format from:

<http://arxiv.org/ps/hep-ph/9502261v1>

This figure "fig4-5.png" is available in "png" format from:

<http://arxiv.org/ps/hep-ph/9502261v1>

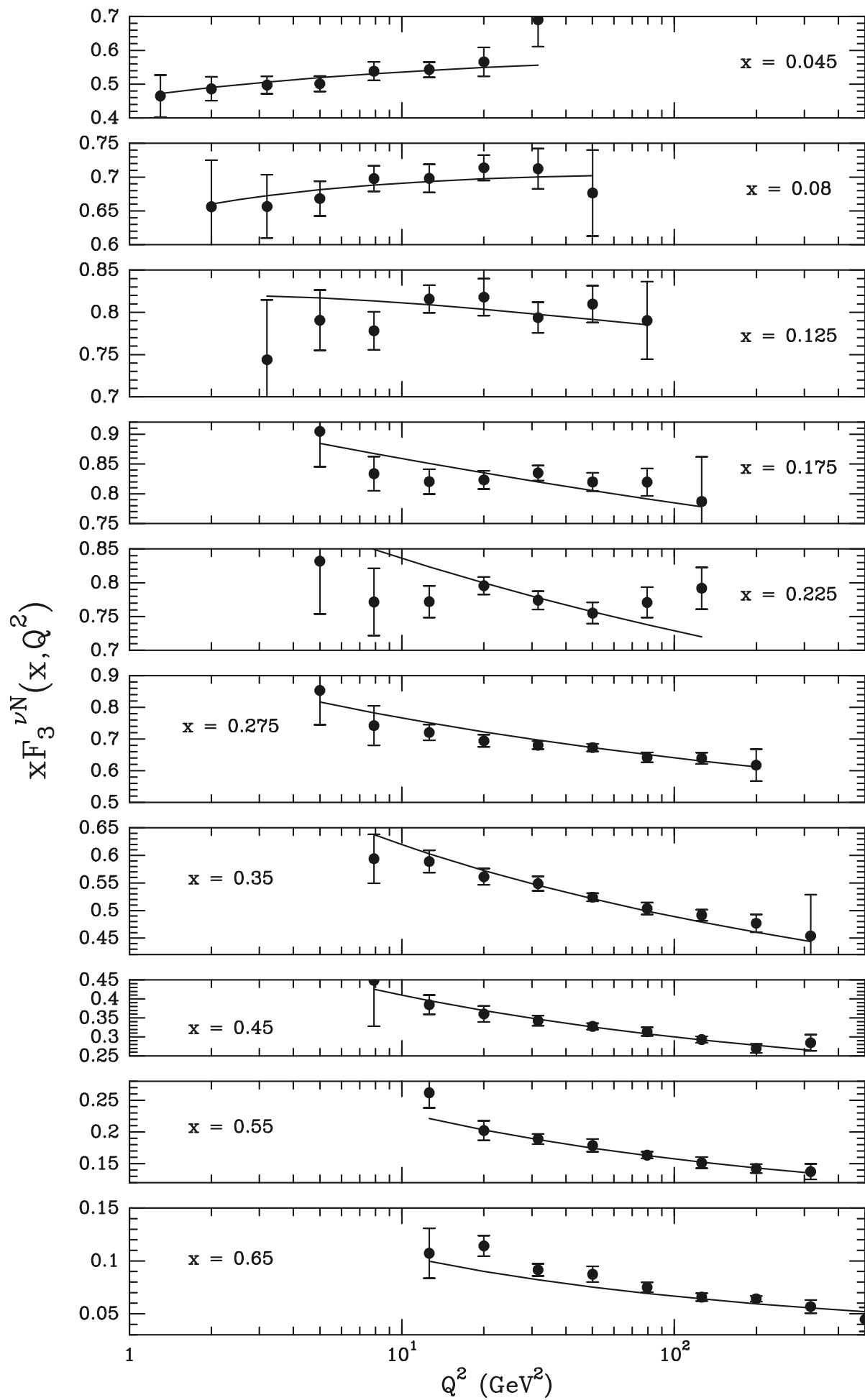


Fig 5

This figure "fig1-6.png" is available in "png" format from:

<http://arxiv.org/ps/hep-ph/9502261v1>

This figure "fig2-6.png" is available in "png" format from:

<http://arxiv.org/ps/hep-ph/9502261v1>

This figure "fig3-6.png" is available in "png" format from:

<http://arxiv.org/ps/hep-ph/9502261v1>

This figure "fig4-6.png" is available in "png" format from:

<http://arxiv.org/ps/hep-ph/9502261v1>

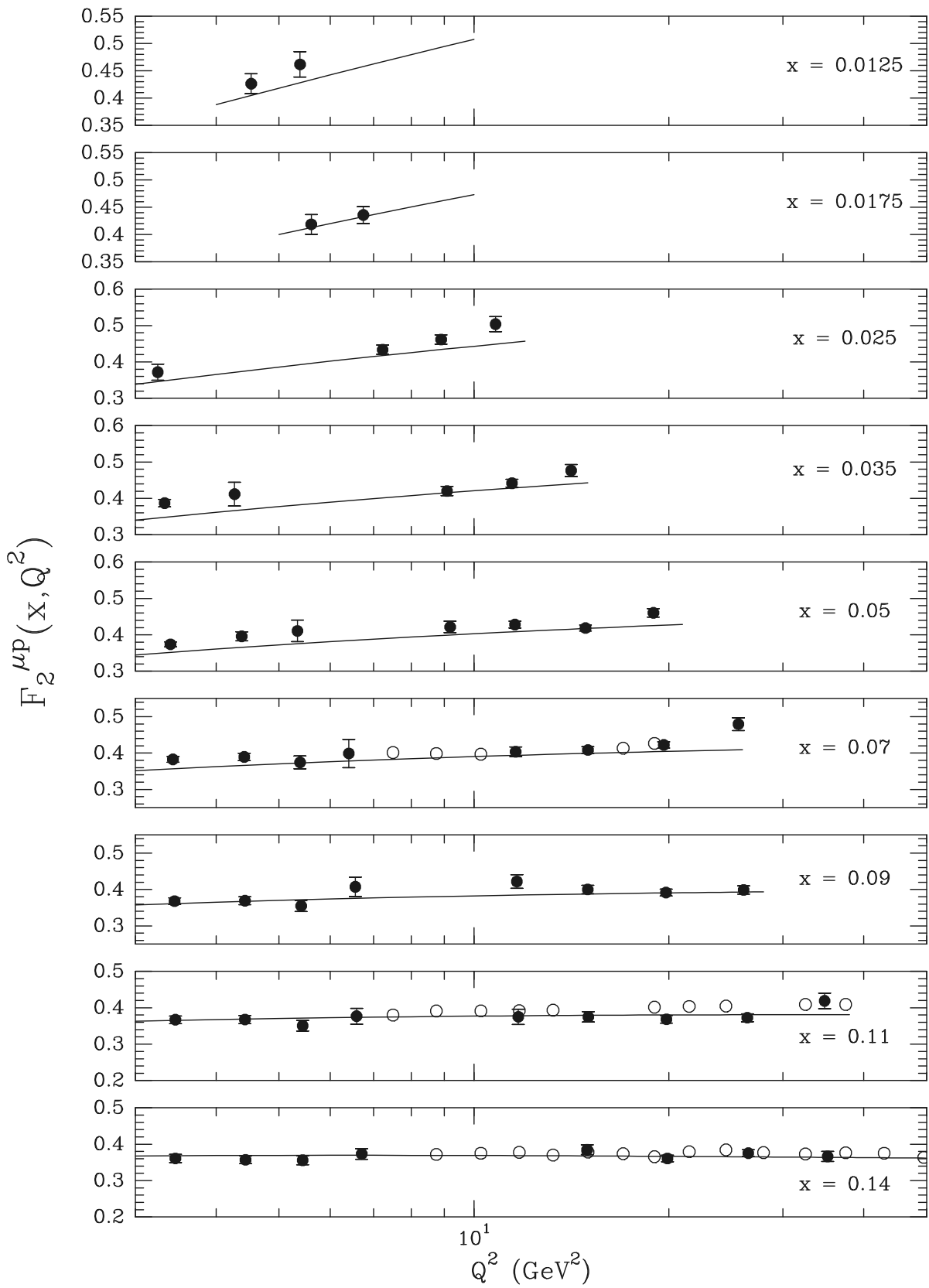


Fig 6a

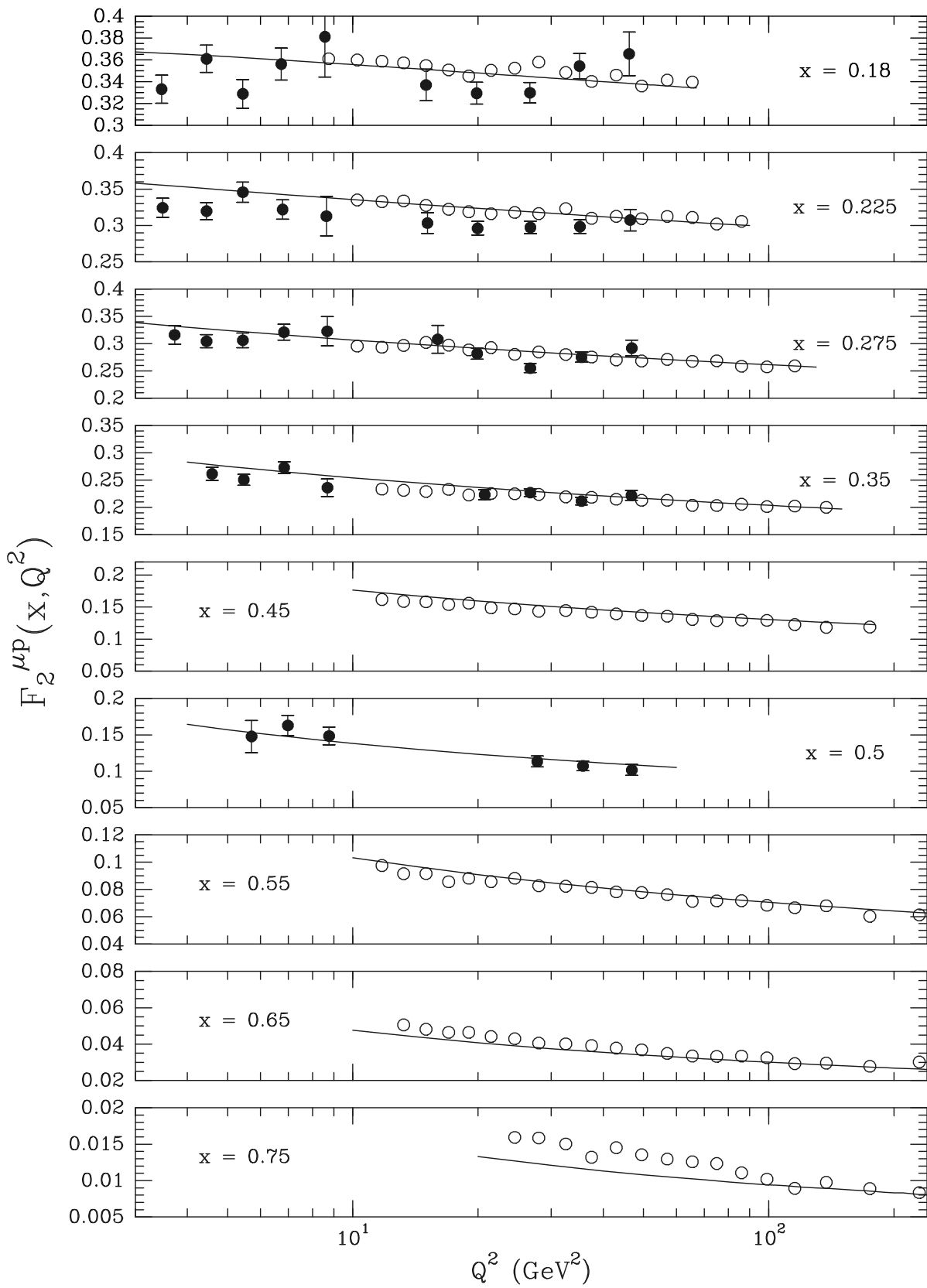


Fig 6b

This figure "fig1-7.png" is available in "png" format from:

<http://arxiv.org/ps/hep-ph/9502261v1>

This figure "fig2-7.png" is available in "png" format from:

<http://arxiv.org/ps/hep-ph/9502261v1>

This figure "fig3-7.png" is available in "png" format from:

<http://arxiv.org/ps/hep-ph/9502261v1>

This figure "fig4-7.png" is available in "png" format from:

<http://arxiv.org/ps/hep-ph/9502261v1>

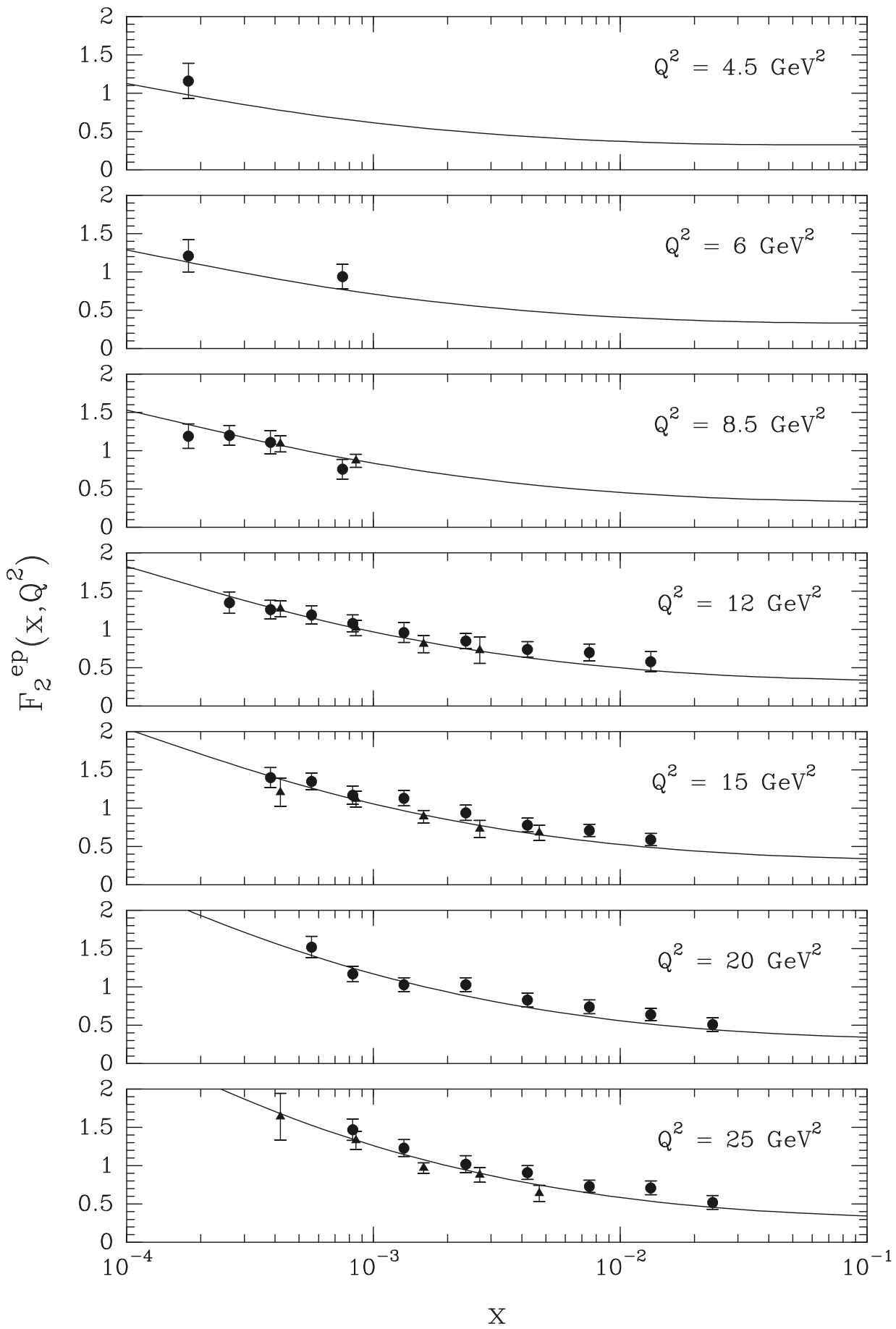


Fig 7a

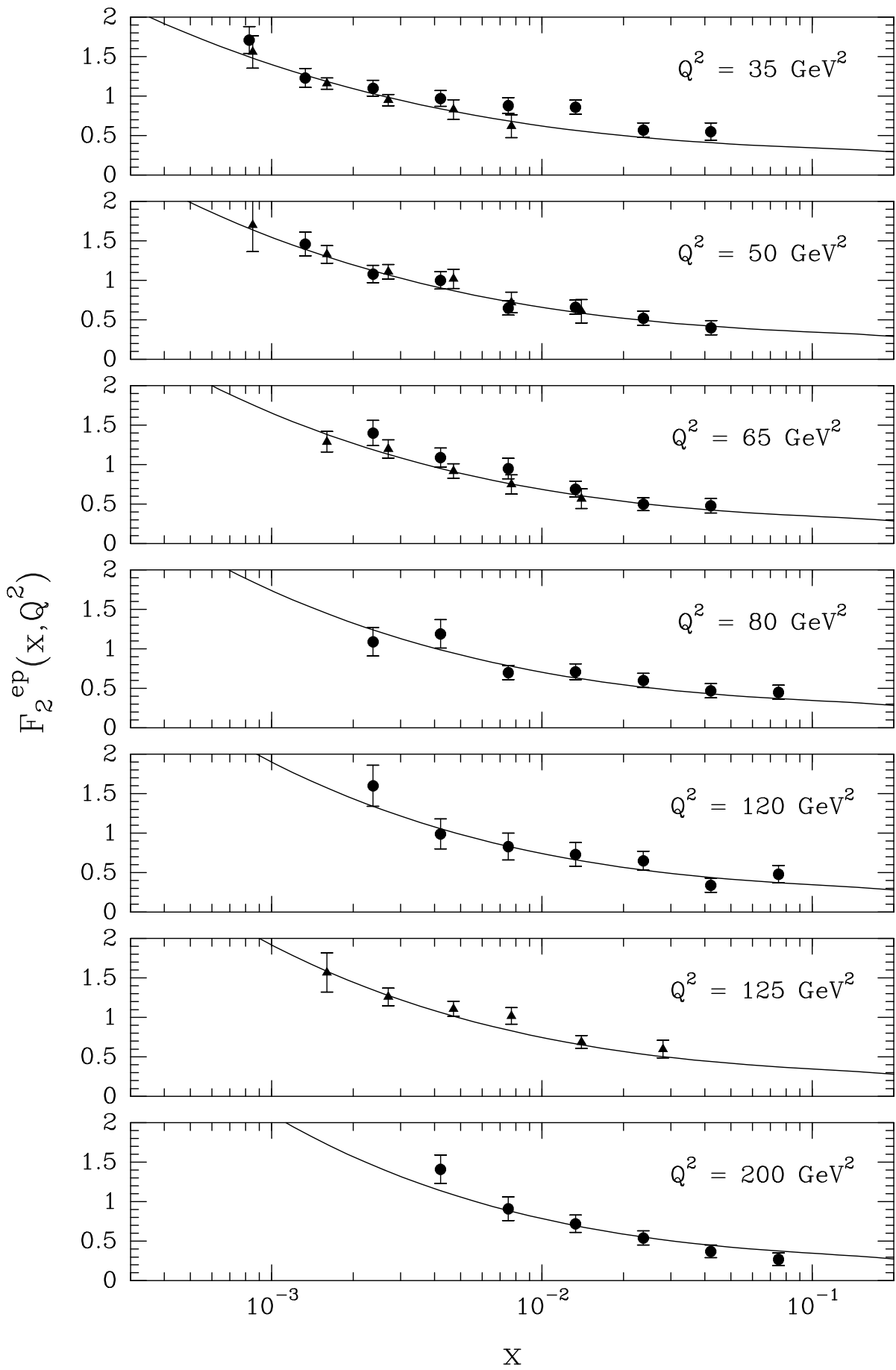


Fig 7b

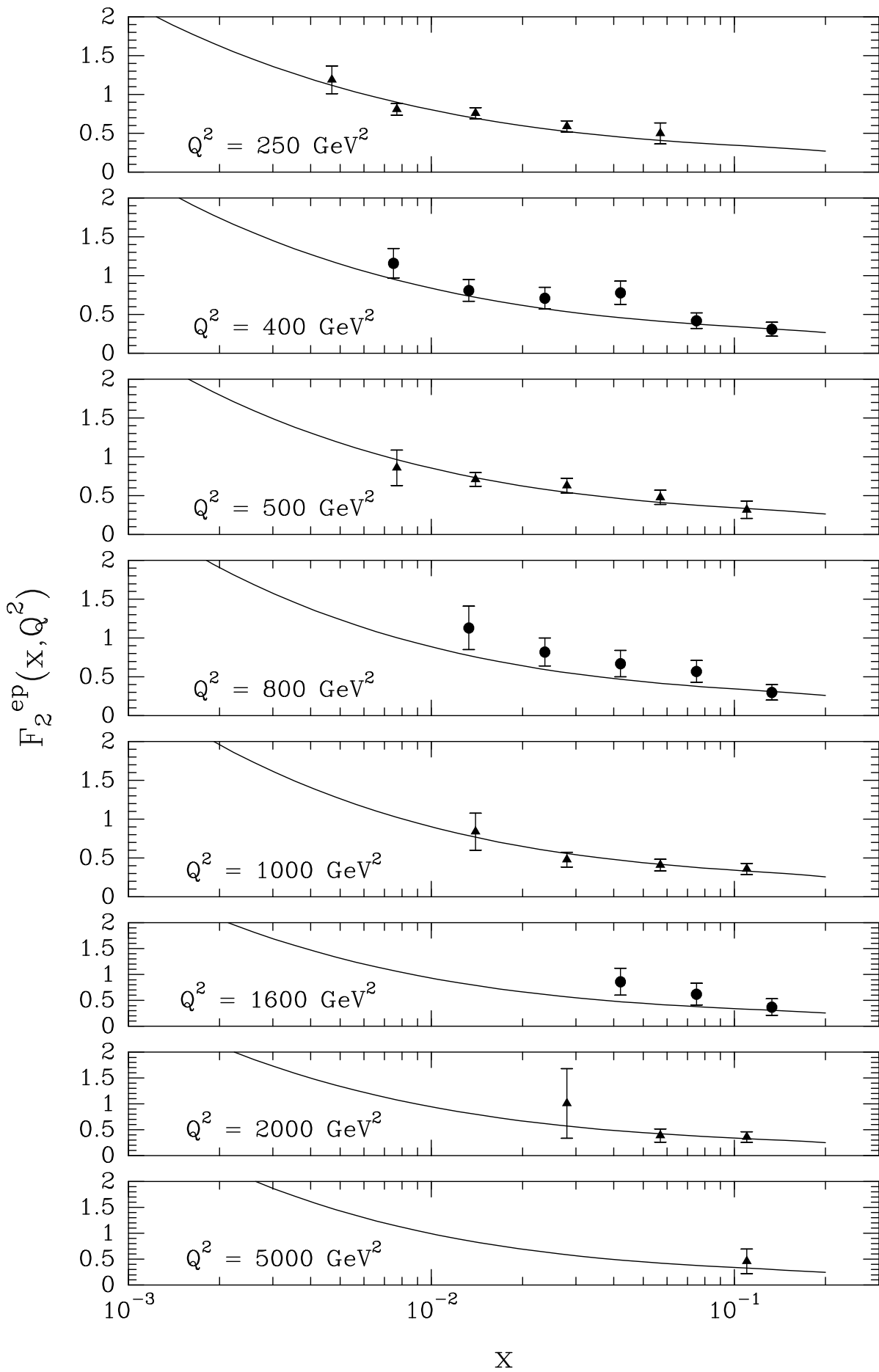


Fig 7c

This figure "fig2-8.png" is available in "png" format from:

<http://arxiv.org/ps/hep-ph/9502261v1>

This figure "fig3-8.png" is available in "png" format from:

<http://arxiv.org/ps/hep-ph/9502261v1>

This figure "fig4-8.png" is available in "png" format from:

<http://arxiv.org/ps/hep-ph/9502261v1>

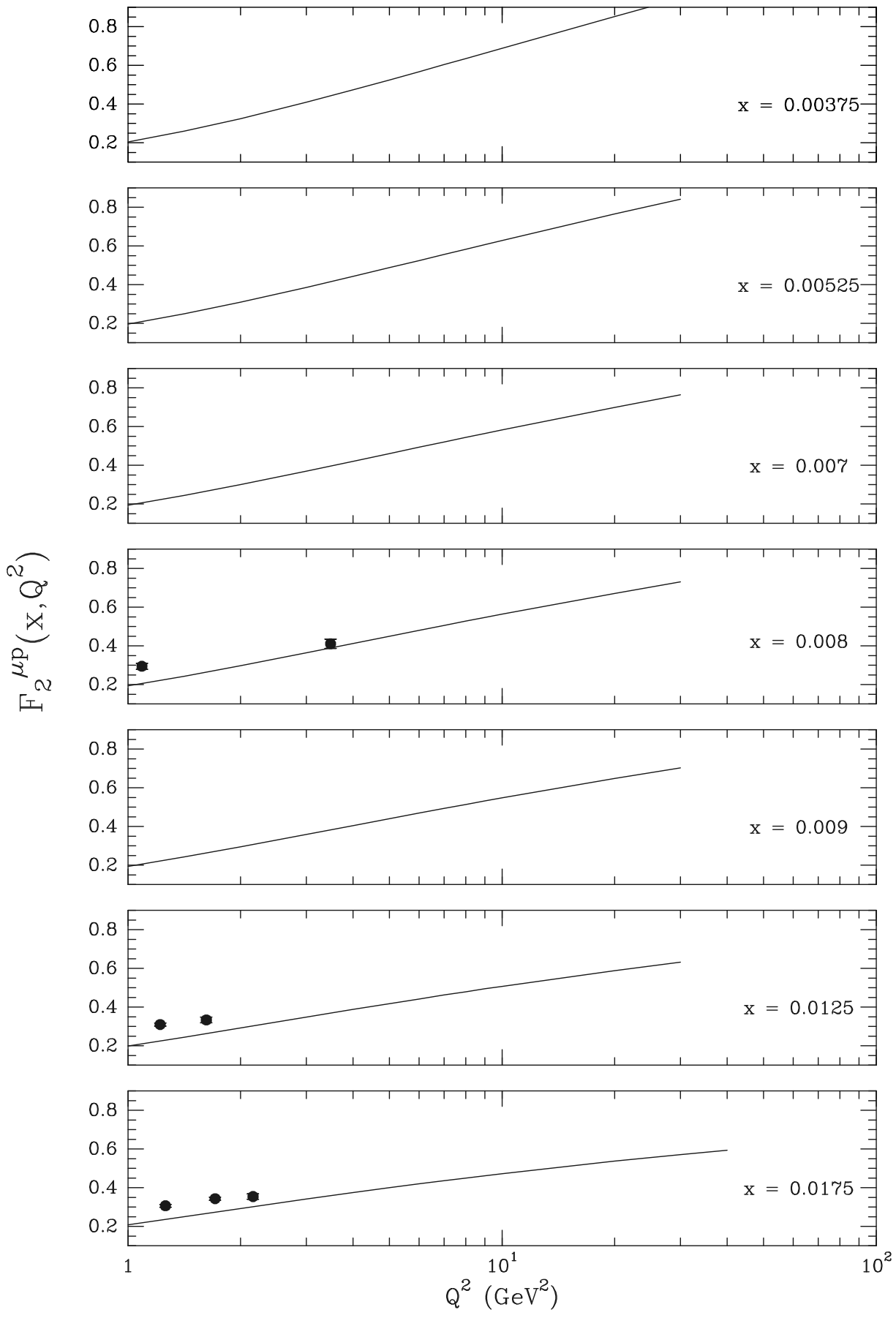


Fig 8a

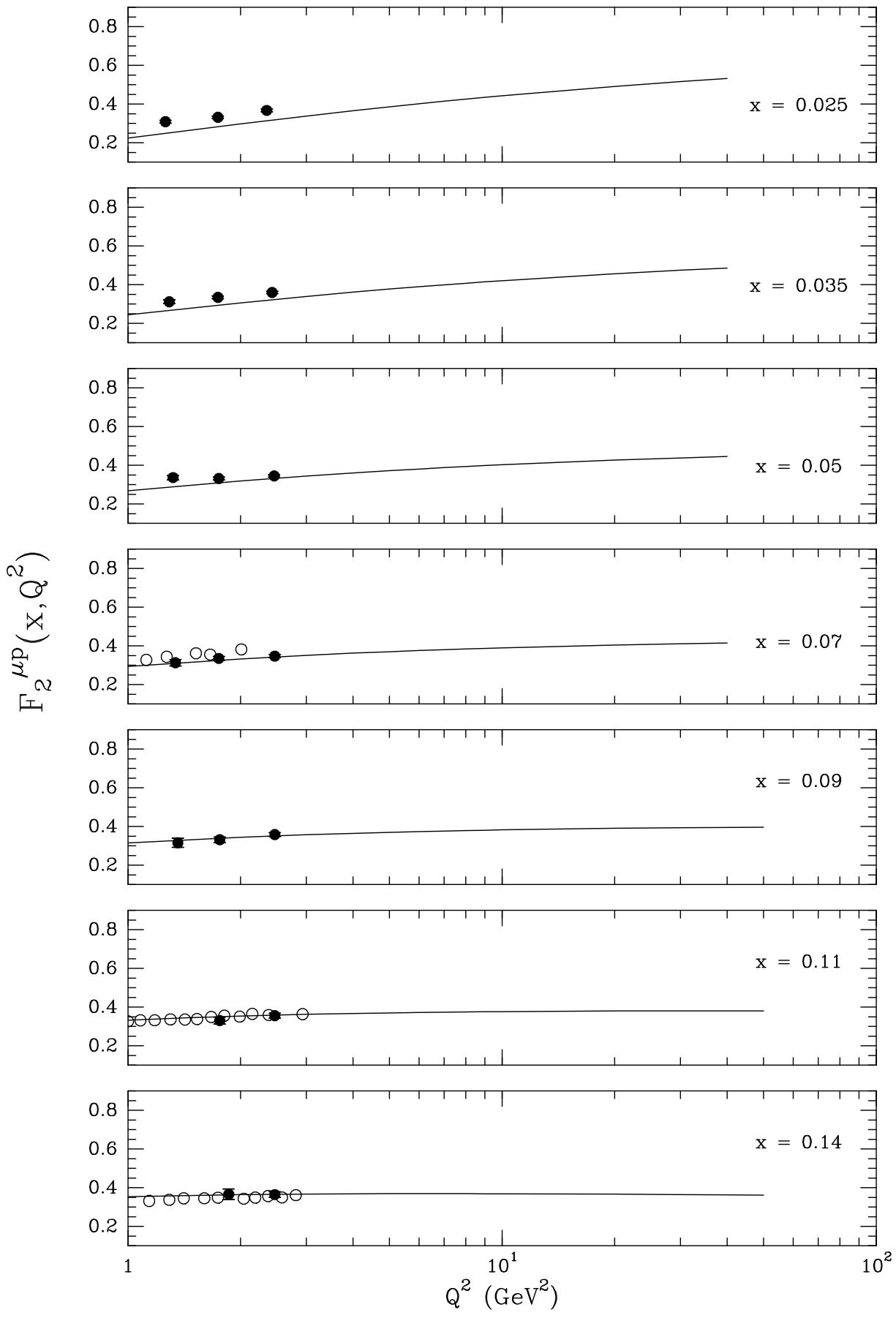


Fig 8b

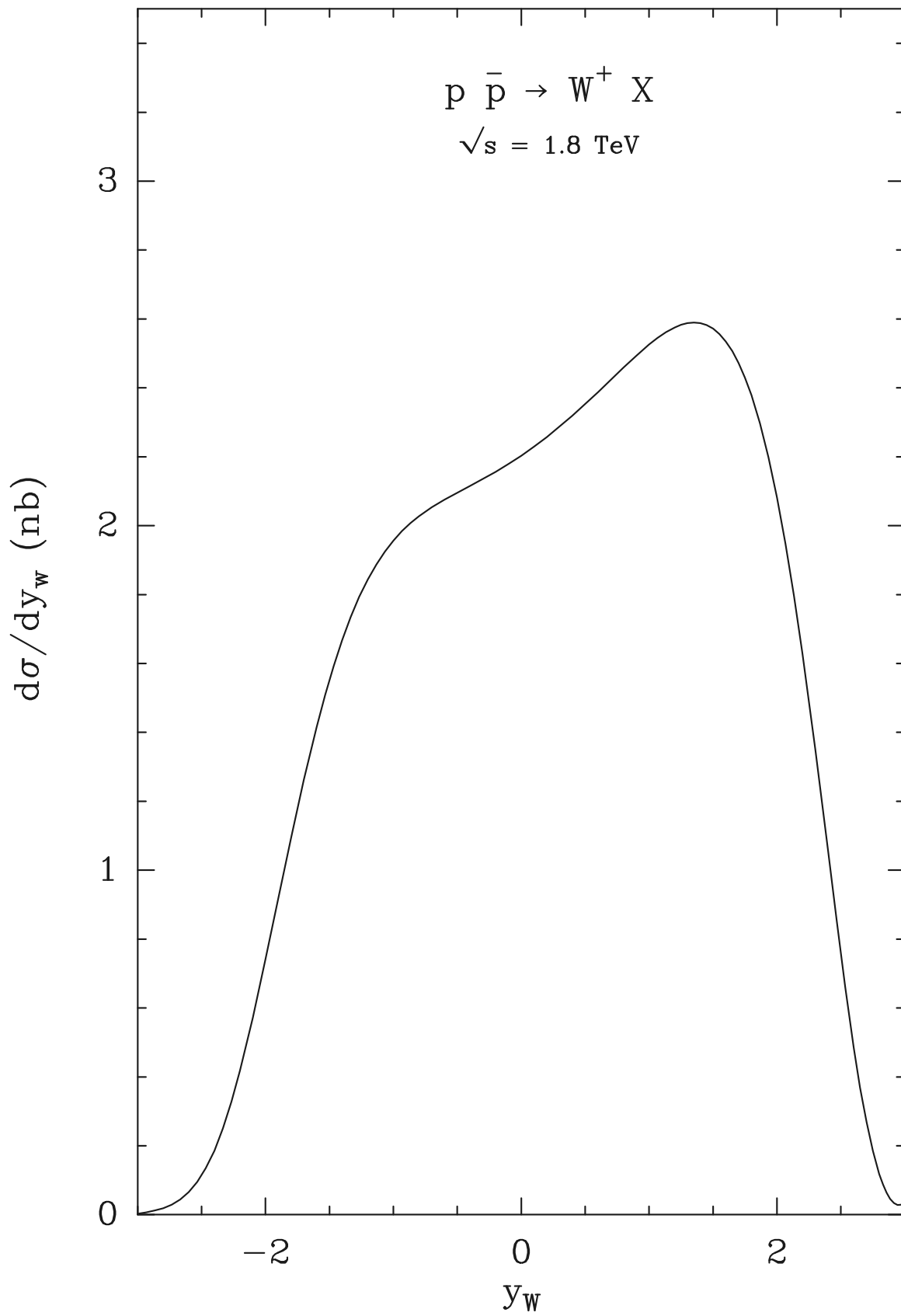


Fig 9

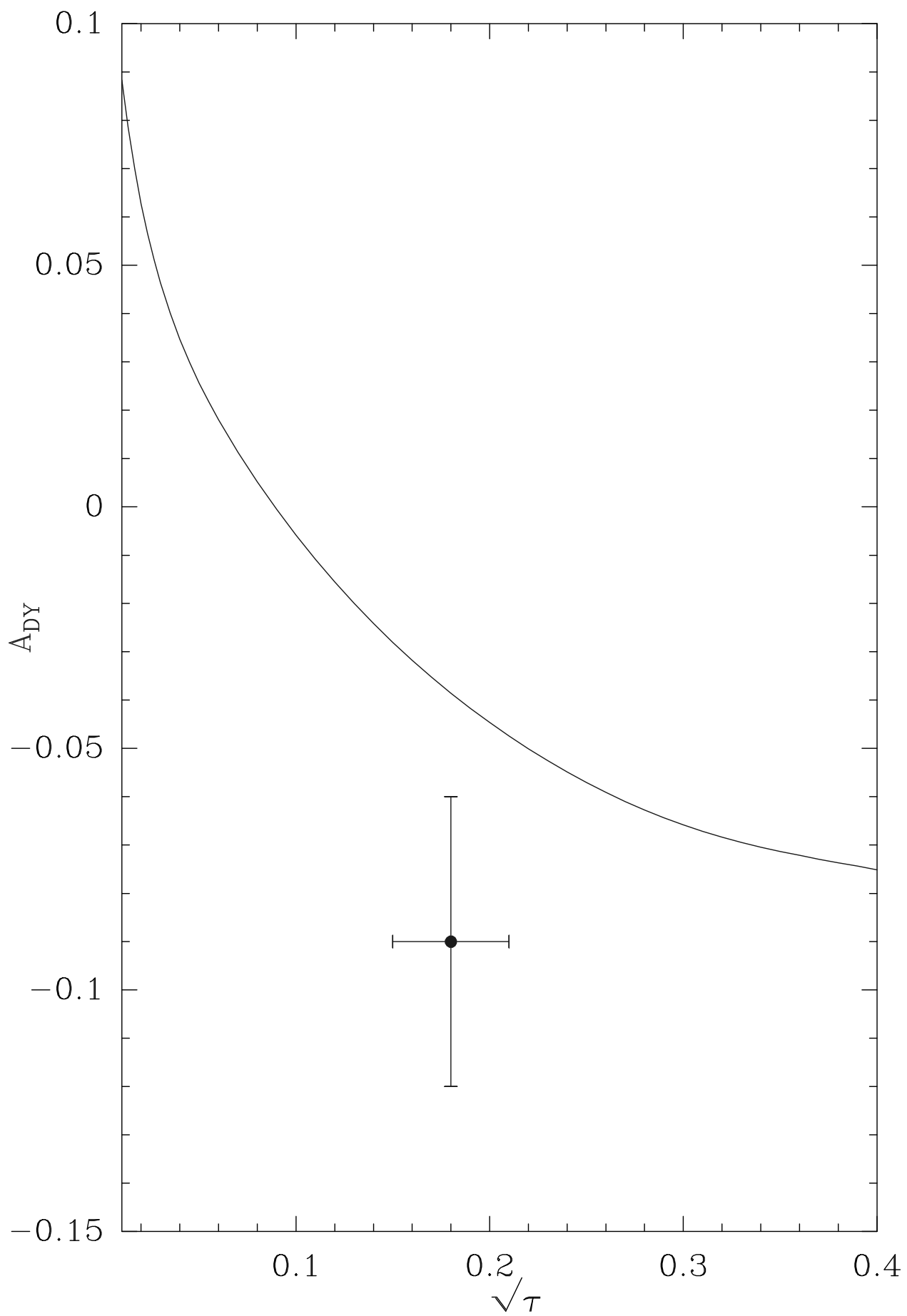


Fig 10

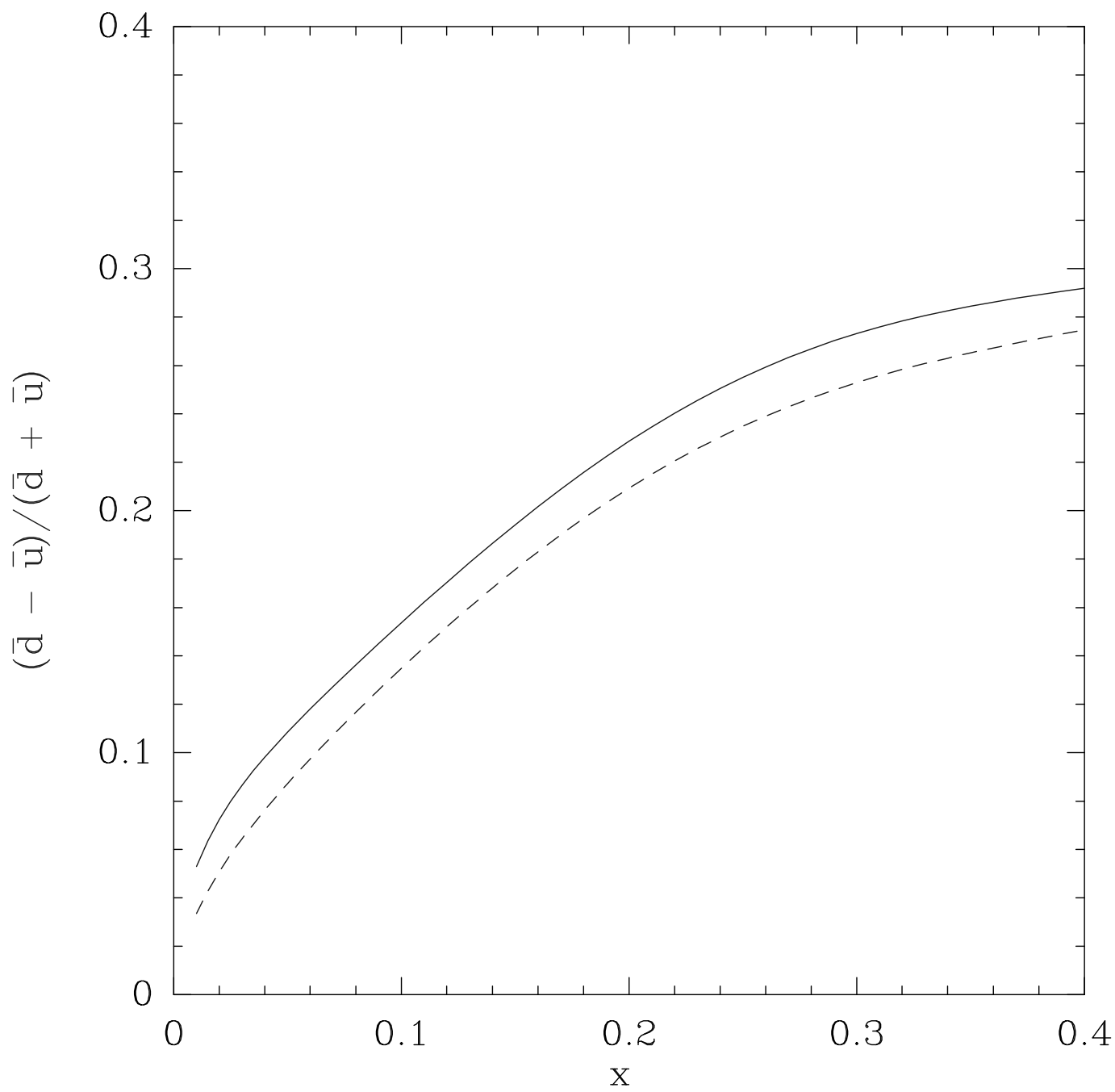


Fig 11

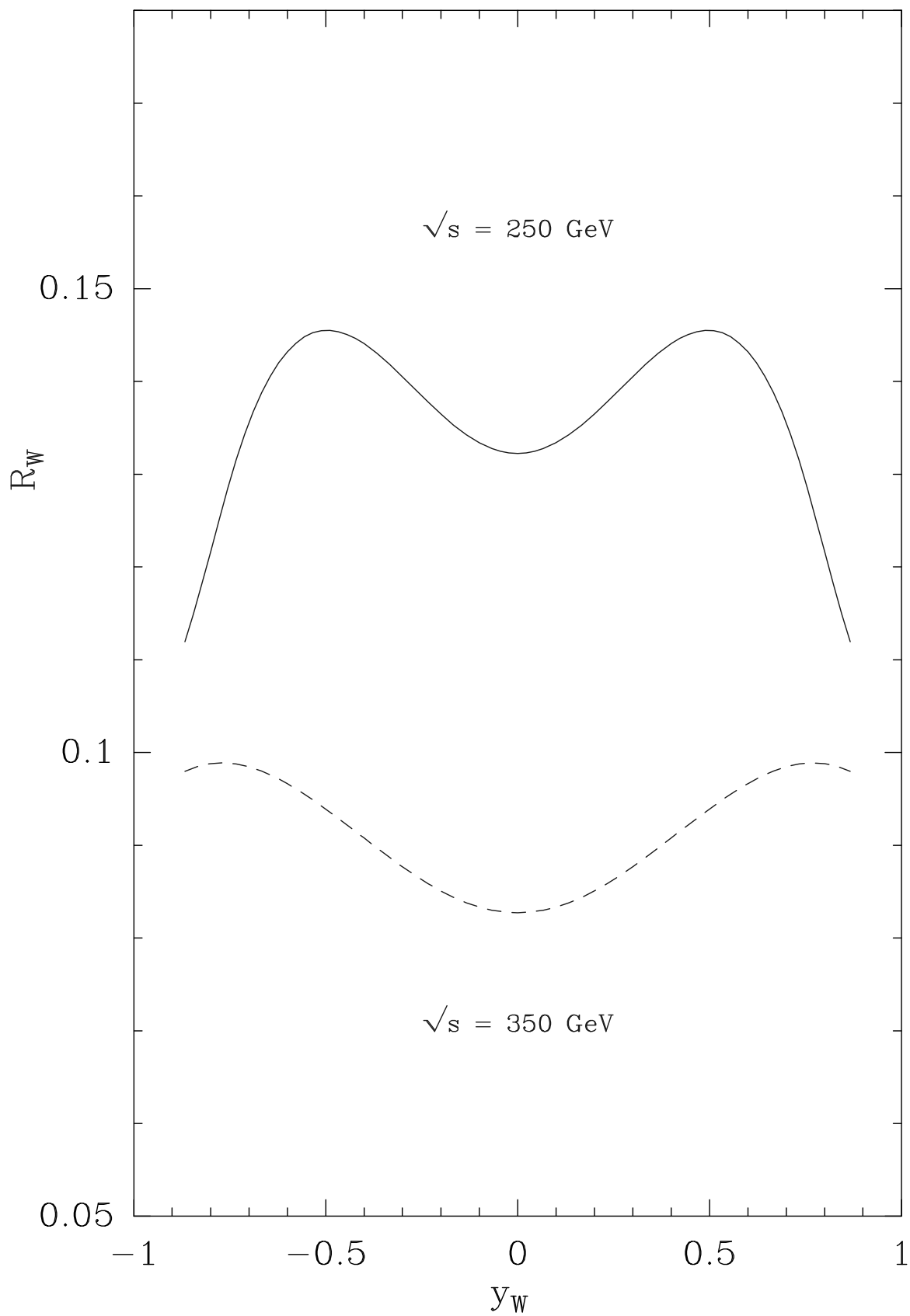


Fig 12

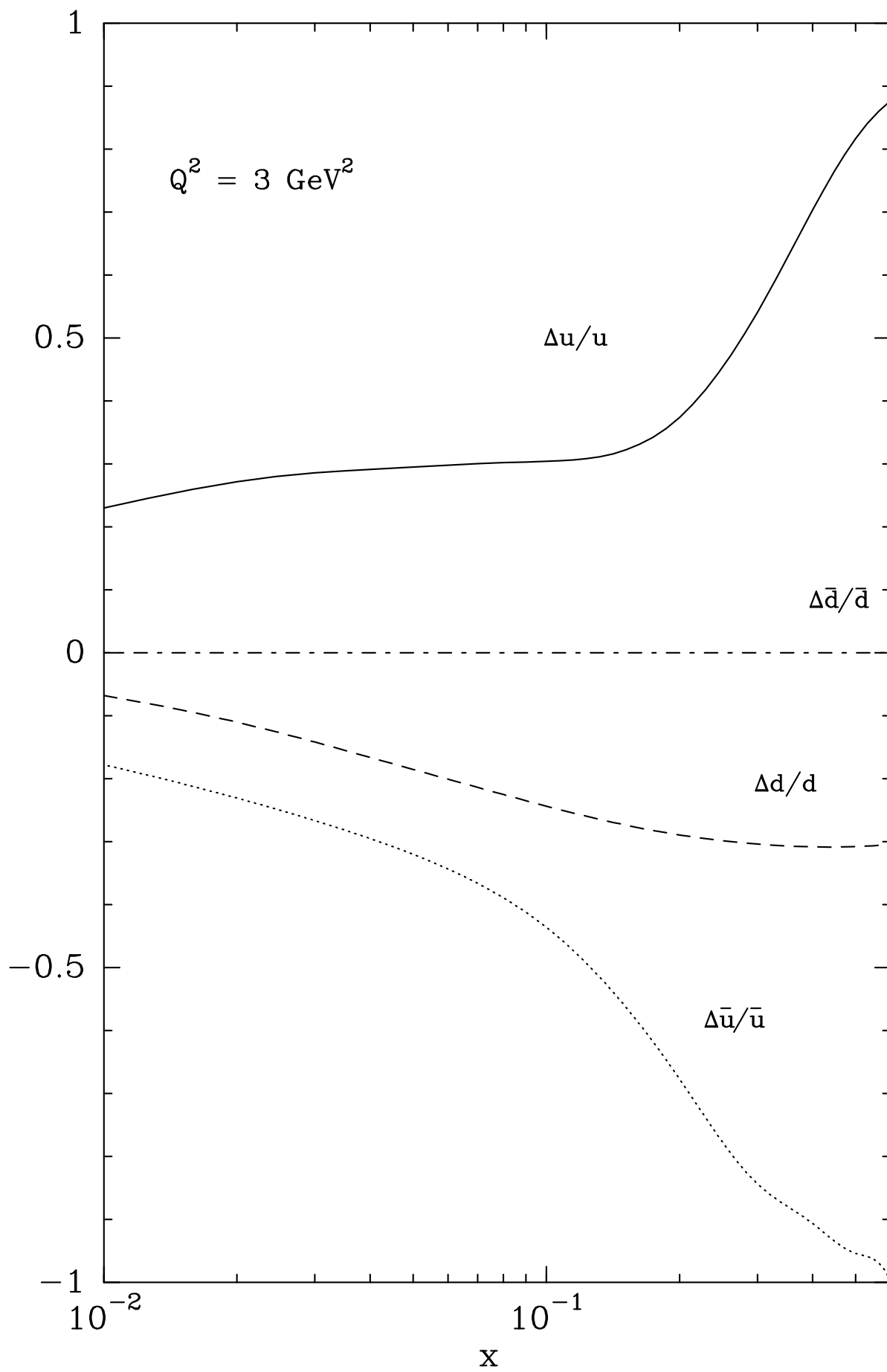


Fig 13

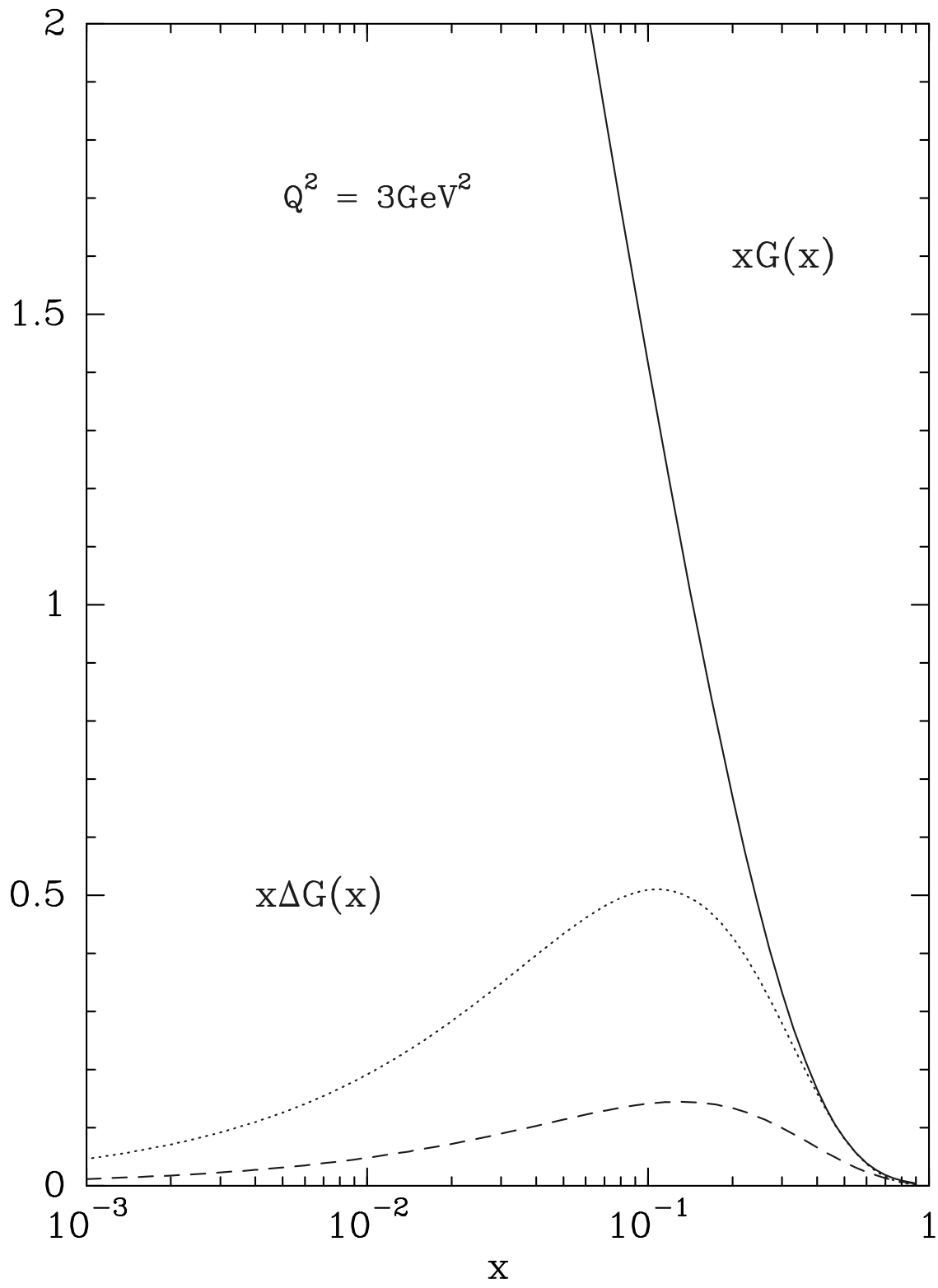


Fig 14

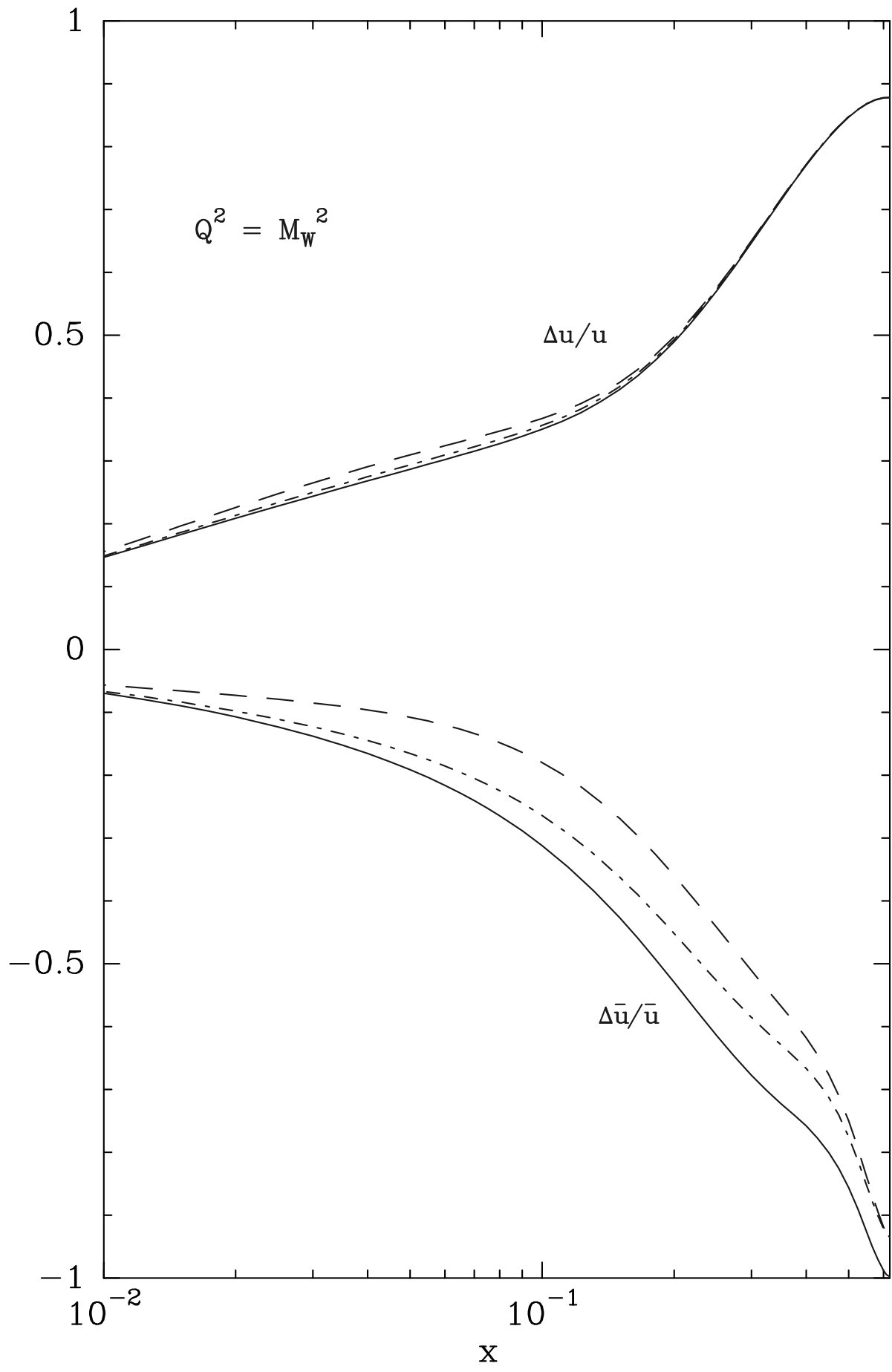


Fig 15a

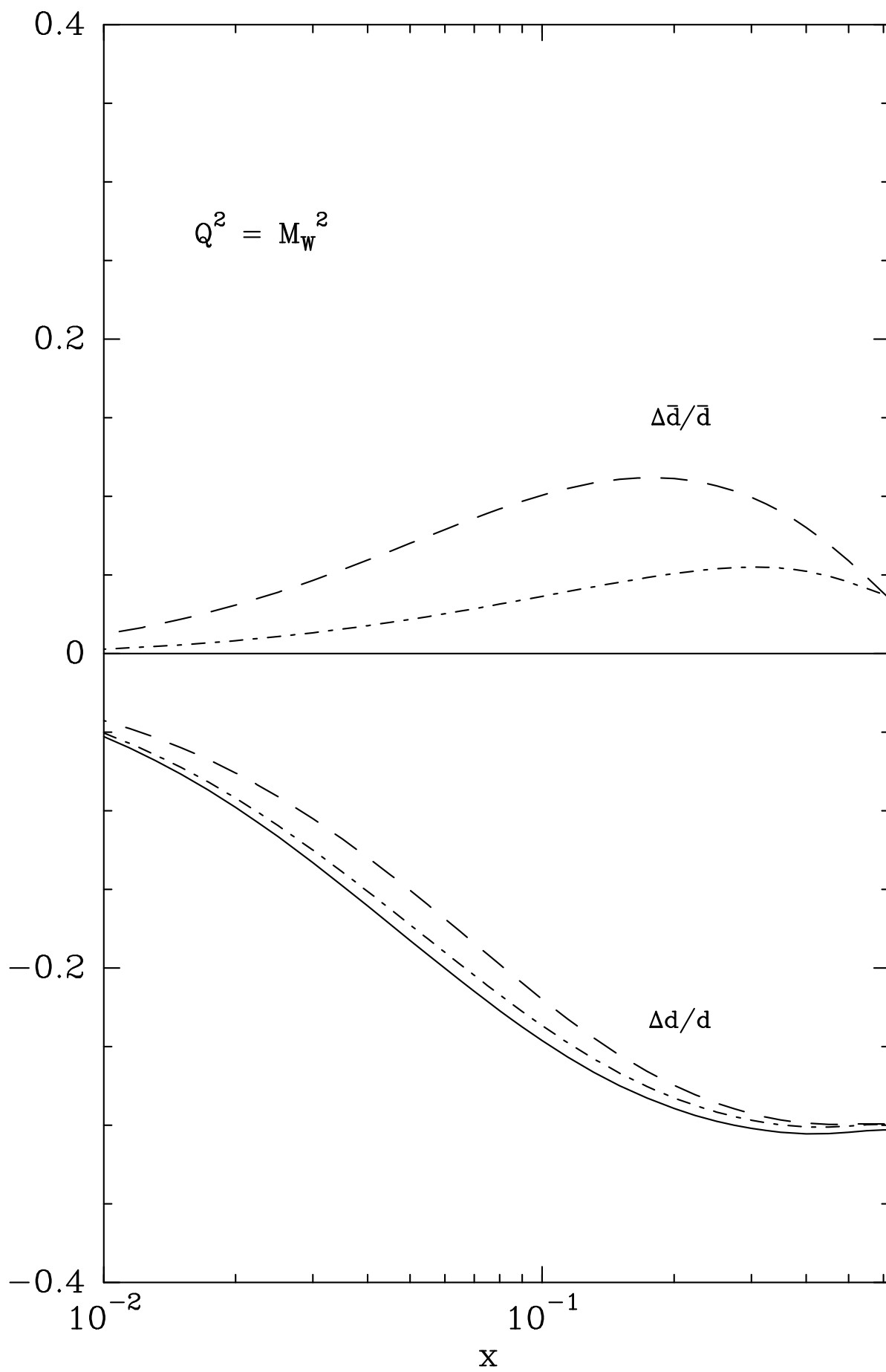


Fig 15b

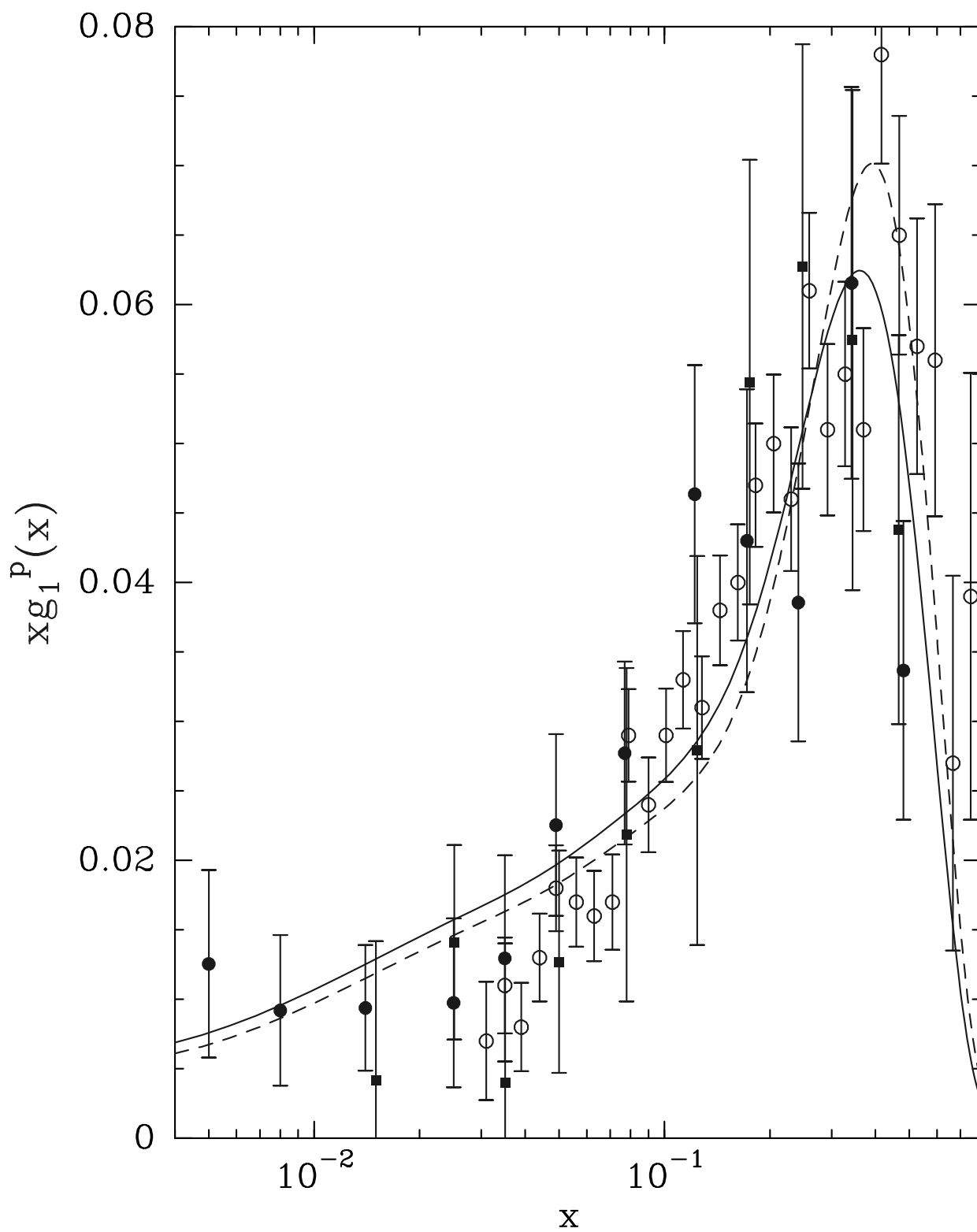


Fig 16

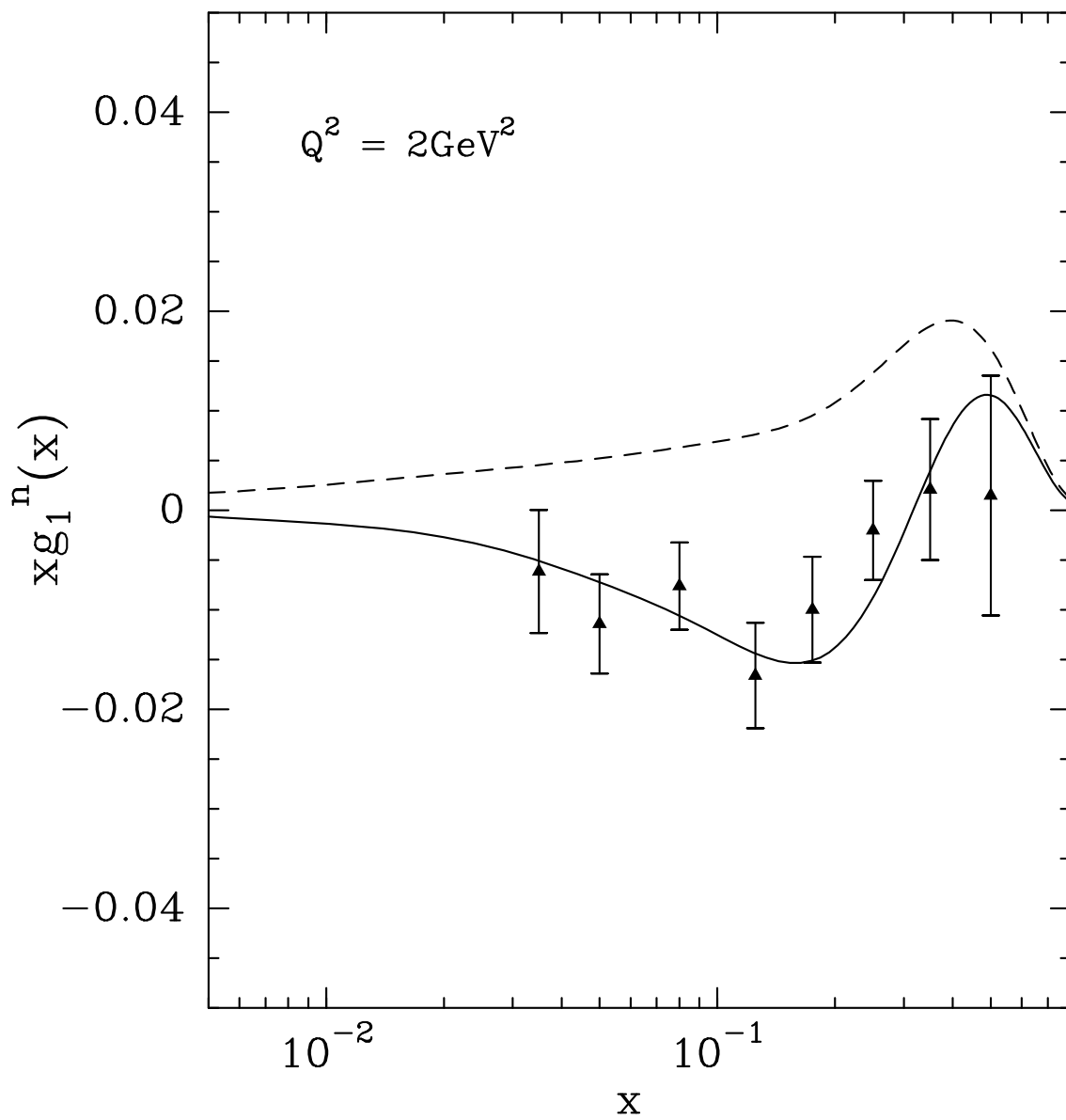


Fig 17

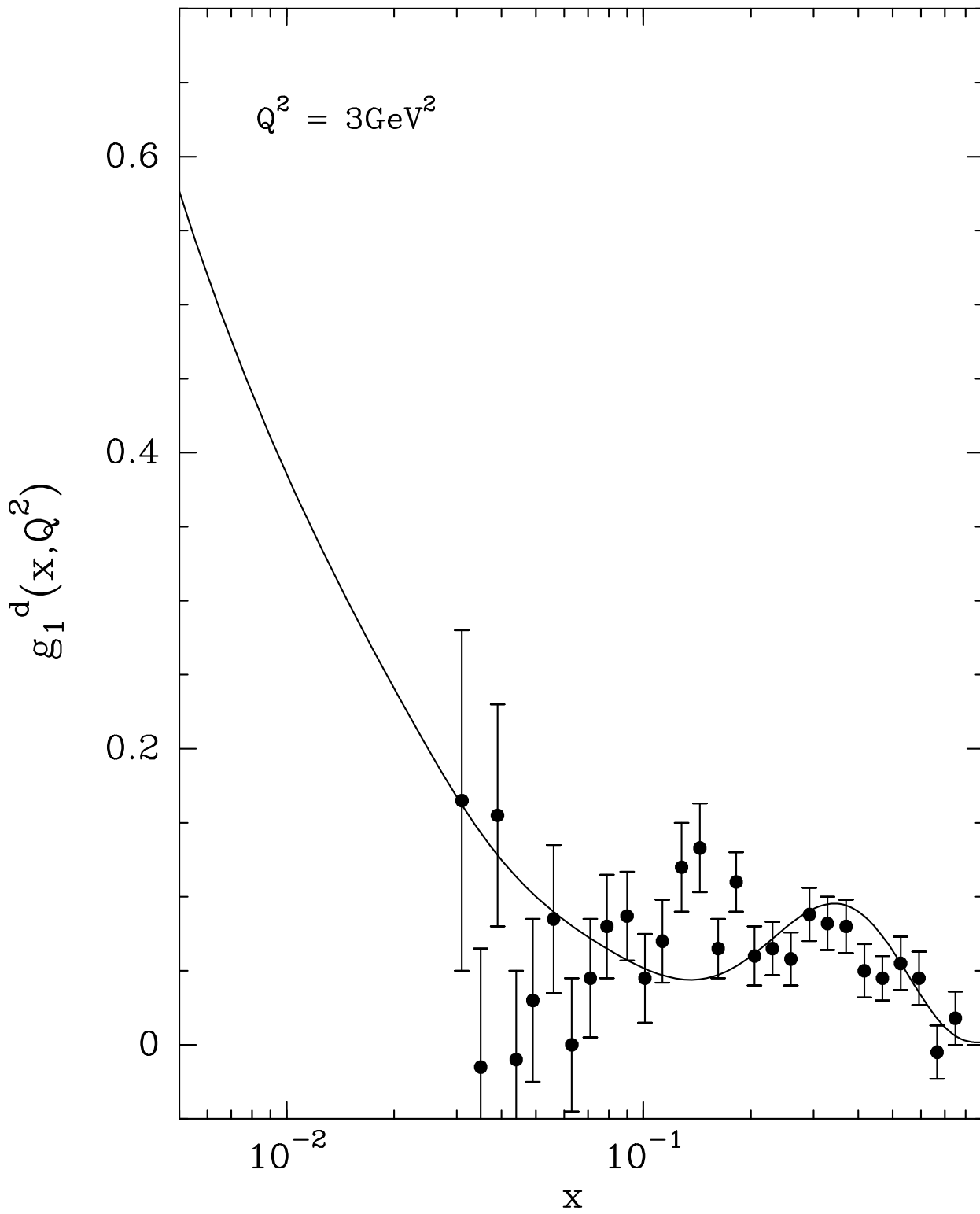


Fig 18

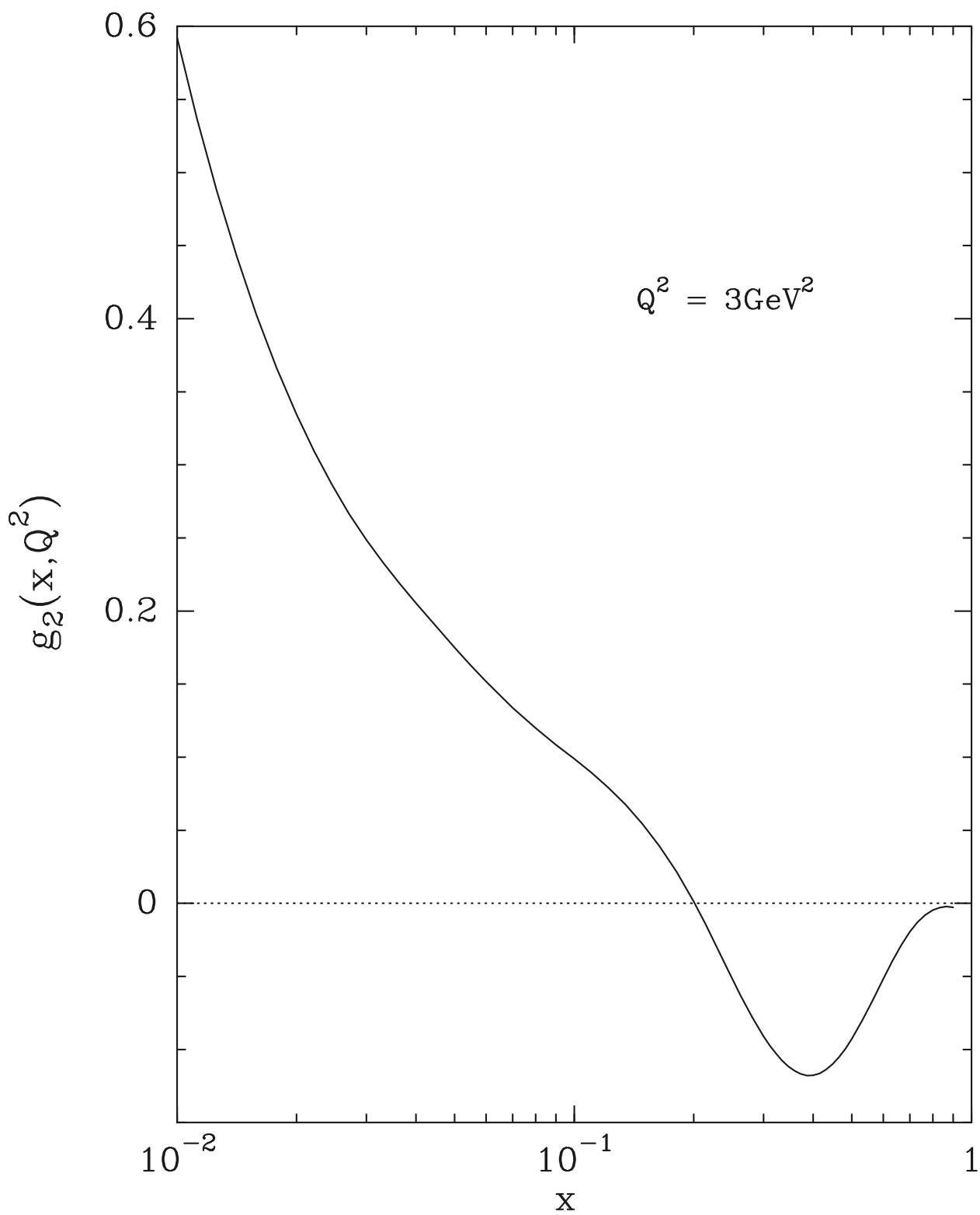


Fig 19

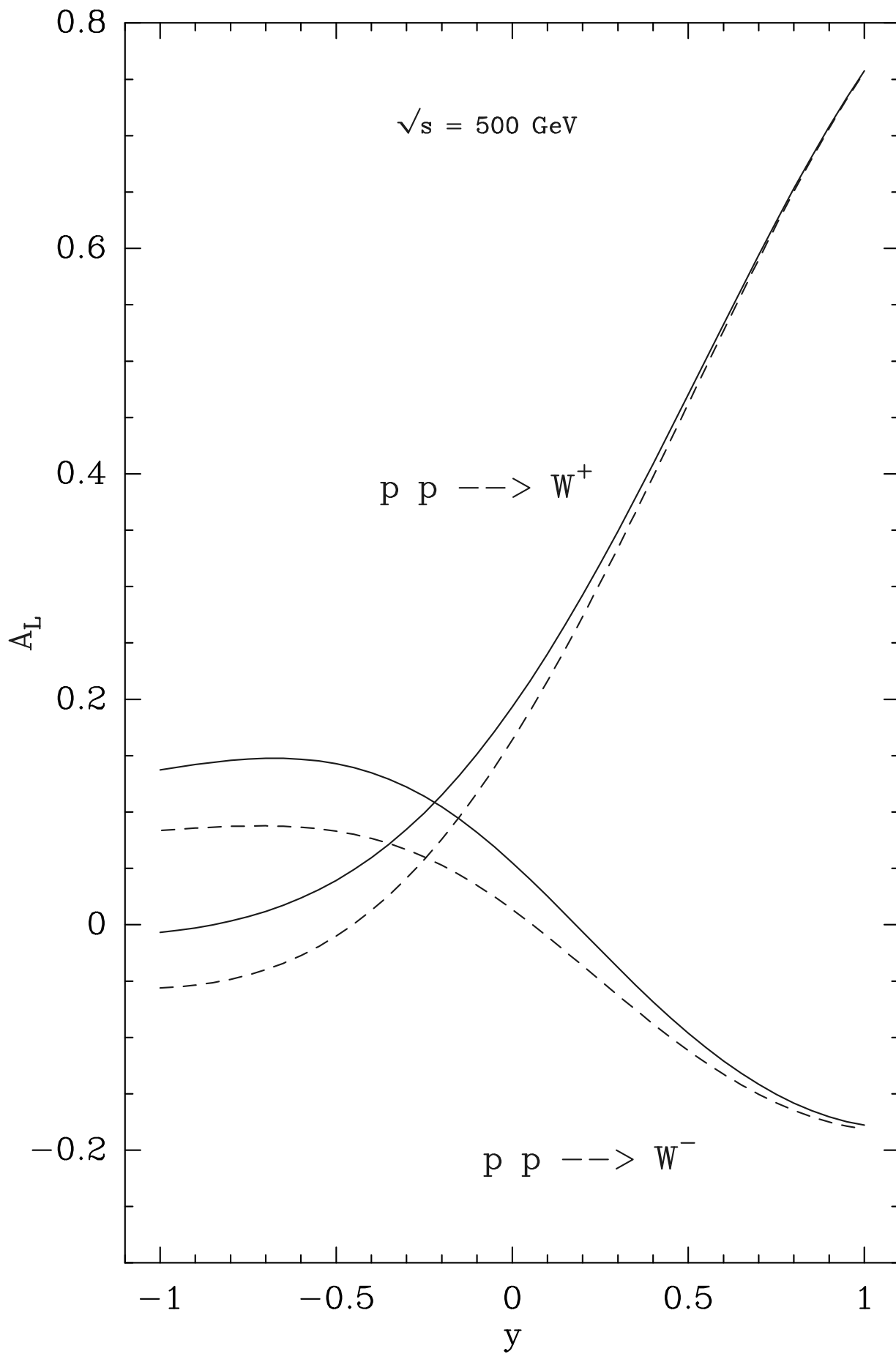


Fig 20

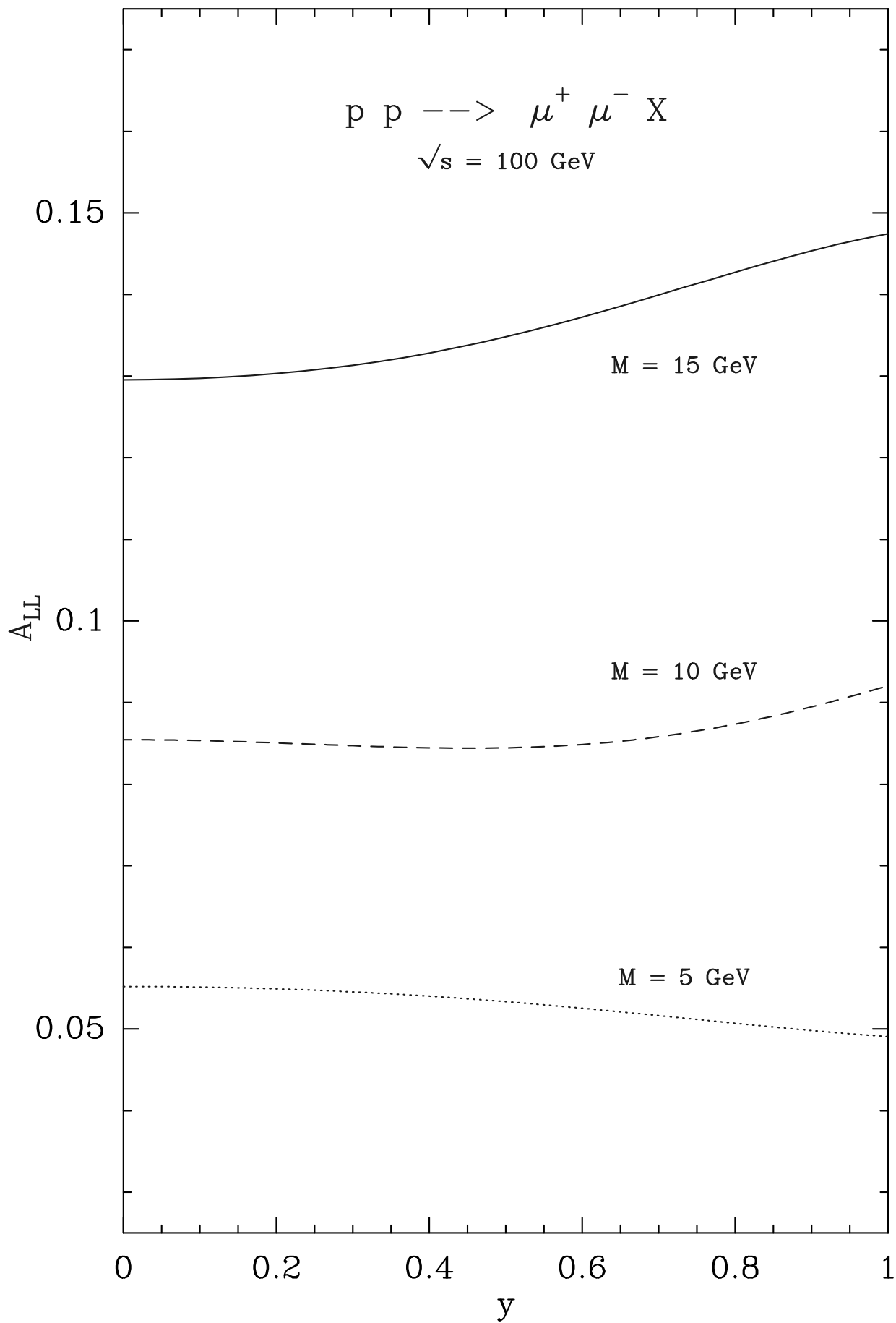


Fig 21

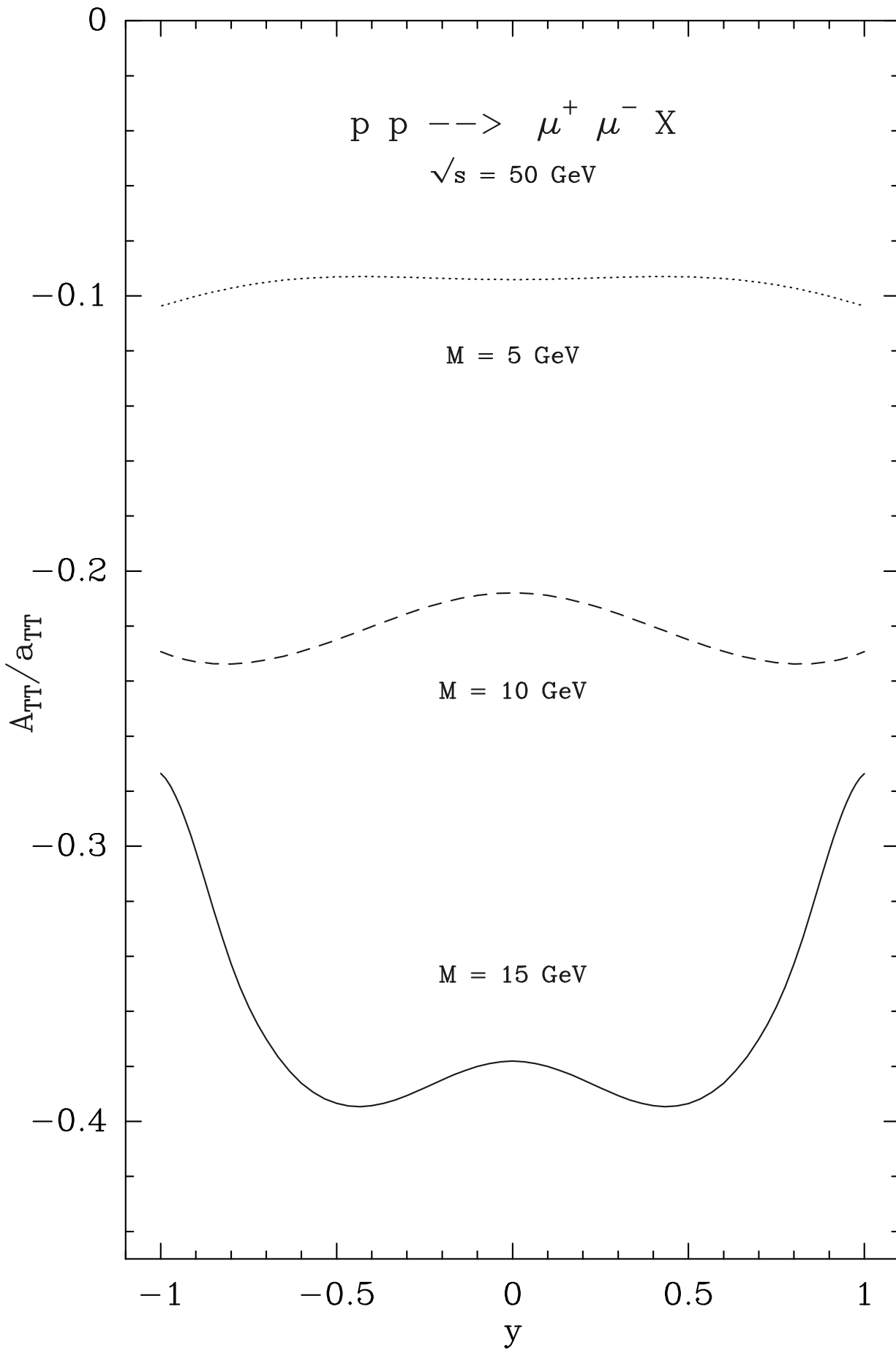


Fig 22a

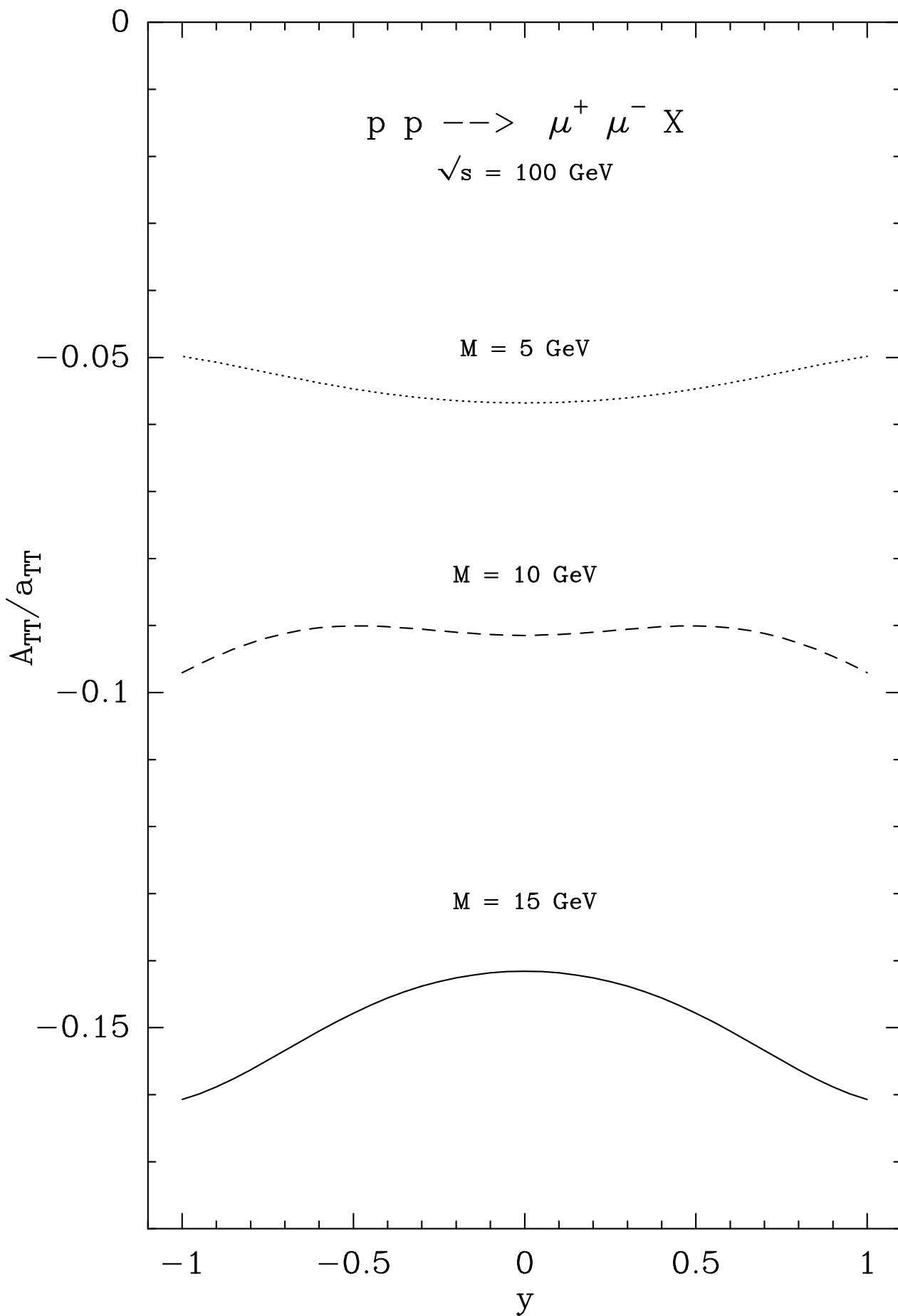


Fig 22b

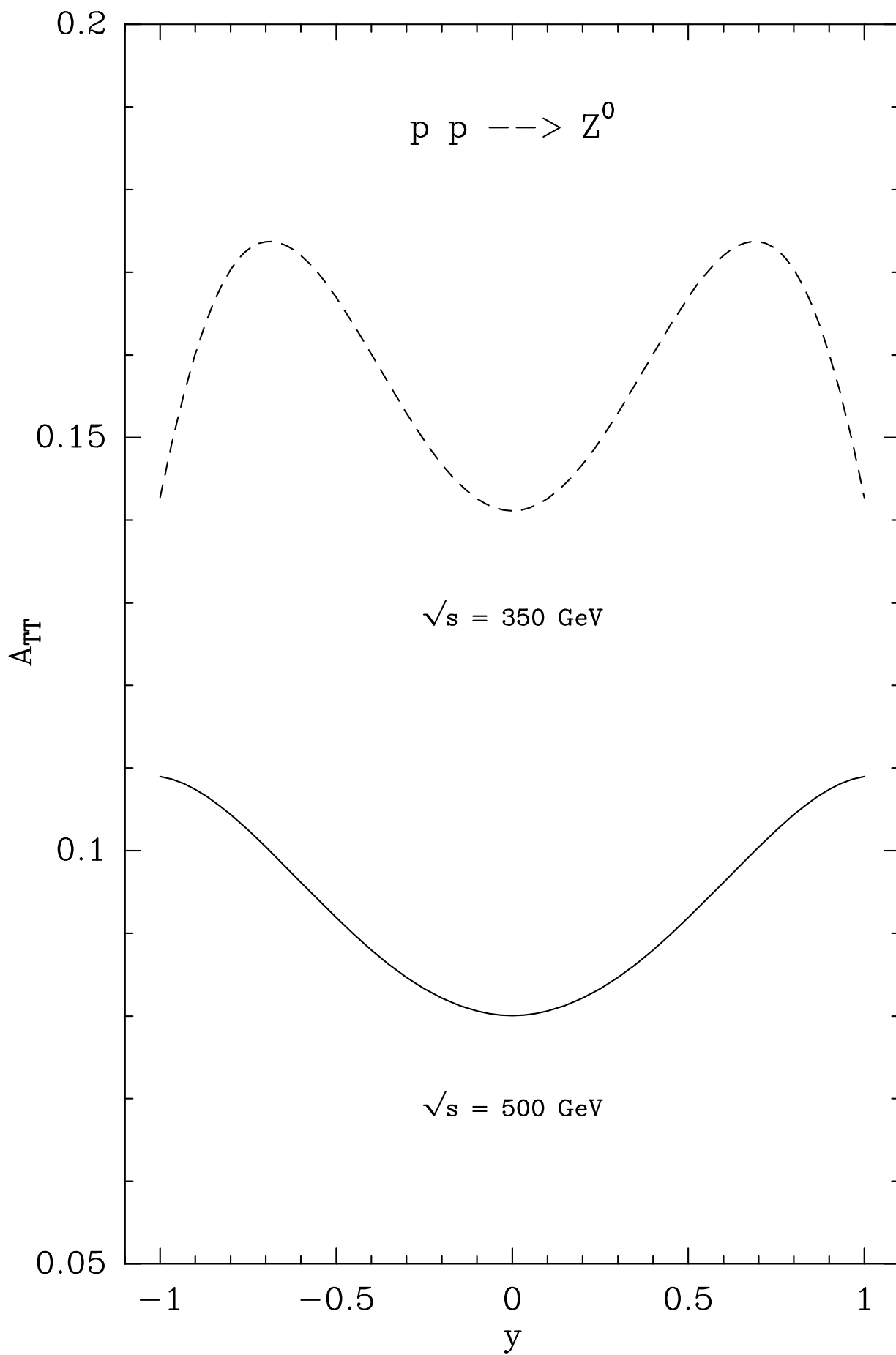


Fig 23